JACS
JOURNAL OF THE AMERICAN CHEMICAL SOCIETY
Article
Cite This: J. Am. Chem. Soc. 2019, 141, 10253−10271
pubs.acs.org/JACS

Squeezing All Elements in the Periodic Table: Electron Configuration and Electronegativity of the Atoms under Compression

Martin Rahm,*[,†] Roberto Cammi,[‡] N. W. Ashcroft,[§] and Roald Hoffmann[∥]

[†]Department of Chemistry and Chemical Engineering, Chalmers University of Technology, SE-412 96 Gothenburg, Sweden
[‡]Department of Chemical Science, Life Science and Environmental Sustainability, University of Parma, 43124 Parma, Italy
[§]Laboratory of Atomic and Solid State Physics, Cornell University, Ithaca, New York 14853, United States
[∥]Department of Chemistry and Chemical Biology, Baker Laboratory, Cornell University, Ithaca, New York 14853, United States

Supporting Information

ABSTRACT: We present a quantum mechanical model capable of describing isotropic compression of single atoms in a non-reactive neon-like environment. Studies of 93 atoms predict drastic changes to ground-state electronic configurations and electronegativity in the pressure range of 0−300 GPa. This extension of atomic reference data assists in the working of chemical intuition at extreme pressure and can act as a guide to both experiments and computational efforts. For example, we can speculate on the existence of pressure-induced polarity (red-ox) inversions in various alloys. Our study confirms that the filling of energy levels in compressed atoms more closely follows the hydrogenic *aufbau* principle, where the ordering is determined by the principal quantum number. In contrast, the Madelung energy ordering rule is not predictive for atoms under compression. Magnetism may increase or decrease with pressure, depending on which atom is considered. However, Hund's rule is never violated for single atoms in the considered pressure range. Important (and understandable) electron shifts, s→p, s→d, s→f, and d→f are essential chemical and physical consequences of compression. Among the specific intriguing changes predicted are an increase in the range between the most and least electronegative elements with compression; a rearrangement of electronegativities of the alkali metals with pressure, with Na becoming the most electropositive s^1 element (while Li becomes a p group element and K and heavier become transition metals); phase transitions in Ca, Sr, and Ba correlating well with s→d transitions; spin-reduction in all d-block atoms for which the valence d-shell occupation is d^n ($4 \leq n \leq 8$); d→f transitions in Ce, Dy, and Cm causing Ce to become the most electropositive element of the f-block; f→d transitions in Ho, Dy, and Tb and a s→f transition in Pu. At high pressure Sc and Ti become the most electropositive elements, while Ne, He, and F remain the most electronegative ones.

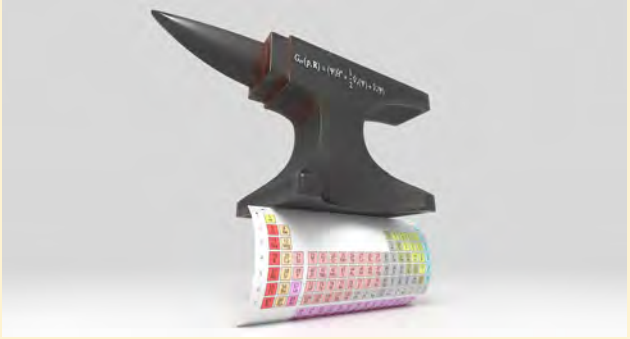

INTRODUCTION

We present a quantum-mechanical model capable of studying the effect of what we will introduce as uniform compression as registered by single *atoms* in a non-reactive medium. Elements 1−96 (with three exceptions to be discussed) up to 300 GPa are examined, following for them two main characteristics: first, the electronic configuration of the ground-state isolated atoms, which arguably defines the very nature of the periodic table; and second, the central chemical notion of electronegativity, so useful for rationalizing chemical bonding and, in particular, making sense of processes involving polarity and charge transfer.

The justification for exploring these quantities at higher than ambient Earth conditions comes from experiment. Today static pressures of hundreds of gigapascals are achievable with diamond anvil cells, and still higher, if fleeting, pressures under shock conditions. The application of pressure to chemical elements has proven a treasure trove for the exploration of exotic phenomena, structures, and chemical bonding,[1] and the making of new and remarkable materials such as polymeric nitrogen,[2] quartz-like CO_2,[3] near room temperature superconductors,[4] carbon nanothreads,[5] metallic hydrogen,[6] and many others.[7] A few of these materials are recoverable to ambient earth conditions, but most are not. In the cosmic perspective, 300 GPa is literally mundane; the pressure at the center of Jupiter, for example, said to be 5−10 TPa.[8]

The nature of the elements changes in dramatic fashion with compression. And so does their chemistry. It is natural that our chemical intuition is formed at $p \approx 1$ atm. To guide our thinking, and because multi-electron systems are inherently complex, we often rely on simplifying tools—models and descriptors such as valence electron configuration, frontier orbitals,[9] sizes of the atoms or ions,[10] electronegativity,[11,12]

Received: March 9, 2019
Published: May 30, 2019

DOI: 10.1021/jacs.9b02634
J. Am. Chem. Soc. 2019, 141, 10253−10271

and many others.[13−16] Traditional chemical descriptors, such as these, have also shown themselves useful in the everyday work of not only chemists but physicists and engineers as well. These more or less well-defined indicators also serve as input data for machine-learning approaches aimed at high-throughput material discovery.[17,18] The chemical imagination guides us for some way into the world of highly compressed matter, but even if we remain with ambient pressure chemical descriptors, we need to see how they evolve as the density of matter rises under compression.

The confinement of quantum systems, with remarkable physical consequences, has a long history in the literature. Experimental examples include atom and molecular trapping by, for instance, fullerenes,[19,20] clathrates, and zeolitic channels.[21,22] Semiconductor quantum dots and nanostructures are another illustration of striking confinement effects for chemistry and physics.[23]

The first to consider confinement of an atomic system theoretically were probably Wigner and Seitz, who discussed compression of a sodium atom in a crystalline lattice.[24,25] They were followed by Michels, de Boer, and Bijl, who first considered a hydrogen atom in an impenetrable sphere as a model for compression,[26] and Sommerfeld and Welker.[27,28] More sophisticated calculations along the same lines were later done by Ludena,[29] followed by many others. For a more extensive coverage of the literature and history on confined systems and methodology we refer to the literature, which includes an entire volume of *Advances in Quantum Chemistry*.[30−40]

There are relatively few studies of compressed individual atoms that have actually calculated the pressure from the derivative of the total energy with respect to volume. We already mentioned the pioneering work by Michels et al. on compression of a hydrogen atom to ∼0.5 GPa.[26] Connerade and Semaoune modeled compression of a single Cs atom using relativistic Dirac−Fock calculations up to a pressure of ∼10 GPa.[41]

The number of studies of confined atoms that shed light on trends in the periodic table is limited. Connerade, Dolmatov, and Lakshmi have published an insightful paper on the valence orbitals occupation of row 4 and 5 alkali, alkaline earth and transition metal atoms, and discussed changes in their s-d occupation arising due to compression.[42] One of the conclusions of Connerade et al.'s work is that s-d competition eventually should disappear under compression, so that any two elements in corresponding positions but in different rows of the periodic table will have the same valence electron configuration. In such a situation, in contrast to normal low-pressure condition, the hydrogenic *aufbau* principle is never violated, and the valence level occupation is determined by the principal quantum number. This, as we shall see later, is mostly true, but nonetheless requires some clarification. Connerade and co-workers apparently did not extend their approach to a systematic study of the entire periodic table under compression, as they initially intended.

Dong et al. have uploaded an *arXiv* manuscript that to the best of our knowledge is the closest to being a systematic study of all the elements under pressure (the f-block elements excluded).[43] These researchers studied individual atoms enclosed by an fcc helium lattice, using the so-called helium compression chamber or matrix method,[44,45] We will address the work of Dong et al. in more detail below.

There remains much that is not known about the general behavior of compressed atoms. Here, for instance, is one intriguing question: It is well known that pressure tends to limit or destroy magnetism in condensed materials,[41] but is this echoed in the behavior of individually compressed atoms?

METHODOLOGY

To apply pressure to an individual atom we exploit the eXtreme Pressure Polarizable Continuum Model (XP-PCM) methodology.[46,47] This is an extension to high pressure of a method well-known in chemistry for treating solvent effects, where the solvent is modeled by a polarizable continuous medium. The method also connects with models of embedding atoms or ions in a continuous medium, a jellium.[48−51] In the XP-PCM method, the atom is placed in a void, a cavity inside an external medium transmitting the pressure. The cavity (C) has a variable radius R_C, and the medium is represented as a continuum material distribution characterized in terms of its dielectric permittivity, ε, and its averaged electronic charge distribution, ρ_M, at the given condition of pressure, p. Atom and medium then interact through two main components: electrostatic interaction and the Pauli repulsive interaction. The latter, the Pauli repulsion, models the penetration into the repulsive region of intermolecular potentials between the atom and the external medium, which is a way to think about how pressure is communicated at the microscopic level.

The pressure is increased by decreasing the radius R_C of the spherical cavity with respect to a predefined reference radius R_C^0. As the cavity volume shrinks, the external medium shrinks with it. In other words, with a compression of the cavity there is an increase in the electron density of the surroundings. The Pauli repulsion with the medium increases because of an increased spatial overlap of the electronic distribution of the atom with the electron density of the medium. The augmented repulsion is due both to the shrinking volume of the cavity and to the increase of the electron density of the medium.

The XP-PCM effective electronic Hamiltonian for the atomic system reads

$$\hat{H} = \hat{H}^{o} + \hat{V}_e + \hat{V}_r \tag{1}$$

where H^o is the Hamiltonian of an isolated atom, $\hat{V}_e$ and $\hat{V}_r$ are, respectively, operators representing the long-range electrostatic and the short-range Pauli repulsion interactions with the surrounding environment.[46,47,52,53] The Pauli repulsion operator $\hat{V}_r$ has the form of a penetrable repulsive step potential located at the boundary of the cavity enclosing the molecular solute, and it is written as

$$\hat{V}_r = \int \hat{\rho}(\mathbf{r}) Z_0 \Theta(\mathbf{r})\, d\mathbf{r} \qquad \Theta(\mathbf{r}) = \begin{cases} 0 & \mathbf{r} \in \mathbf{C} \\ 1 & \mathbf{r} \notin \mathbf{C} \end{cases} \tag{2}$$

where $\hat{\rho}(\mathbf{r}) = \sum_i^N \delta(\mathbf{r} - \mathbf{r}_i)$ is the electron density operator (over the N electrons of the molecular system), Z_0 is the height of a barrier potential, and $\Theta(\mathbf{r})$ is a spherical Heaviside unit step function, equal to 0 inside the cavity **C** and 1 outside of it. The height Z_0 of the step barrier reflects how strong the Pauli repulsion between the medium and molecular system's electrons is. Z_0 depends on the mean electron density $\rho_M(p)$ of the external medium at the given pressure p, and on a semi-empirical parameter η.[46]

The pressure is computed as the derivative of the electronic energy of the atom, G_{er}, with respect to the volume V_c of the confining cavity:

$$p = -\frac{\partial G_{er}}{\partial V_c} \tag{3}$$

where the electron energy, G_{er}, is given by

$$G_{er}(p, \mathbf{R}) = \left\langle \Psi \middle| \hat{H}^{o} + \frac{1}{2}\hat{V}_e + \hat{V}_r \middle| \Psi \right\rangle \tag{4}$$

and where the electronic wave function Ψ of the atom can be obtained at any desired quantum chemical level of theory.[54]

DOI: 10.1021/jacs.9b02634
J. Am. Chem. Soc. 2019, 141, 10253−10271

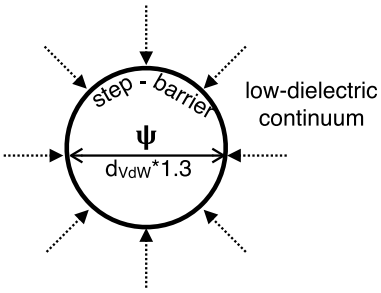

Figure 1. Schematic representation of single-atom compression by a surrounding inert low-dielectric continuum medium of increasing density. An element-characteristic diameter and a confining step barrier define the initial spherical cavities in which elements are placed.

The derivatives of the electronic energy G_{er} for the calculation of pressure p in eq 3 are evaluated by an analytical theory which has been recently developed for XP-PCM by two of the present authors and Bo Chen[55] (see eq 8 in the Supporting Information (SI)). This analytical theory exploits a specific extension of the Hellmann–Feynman theorem[56,57] to the electronic energy G_{er}.[58]

To gauge the volume of the cavity, its radius R_C is expressed as the van der Waals (vdW) radius of the atom times a variable scaling factor f, i.e., $R_C = R_{vdW}f$. An upper value f_0, $R_C^0 = R_{vdW}f_0$, is set in correspondence to near standard condition of pressure ($p < 1$ GPa). To model compression and compare different atoms with each other in a meaningful way, we have used a consistent set of vdW radii[10] available for elements 1–96. These radii mark the average distance from the nuclei where the electron density falls to a value of 0.001 e bohr^{-3} and have been physically justified by their agreement with crystallographically determined vdW radii.[59,60] A radius 30% larger than that set is used to construct the reference radii of the cavities ($R_C^0 = R_{vdW}f_0$; $f_0 = 1.3$). This specific choice was made after tests across the elements of the periodic table assured us that it would provide near-vacuum (<1 GPa) conditions (Figure 1).

To increase the pressure, the cavity scaling factor f is decreased. The cavity scaling factor f also affects the physical parameters of the medium—the dielectric permittivity ε, the electron density ρ, and the Pauli repulsion step barrier Z_0—in the following way:

$$\rho_M(f) = \frac{\rho_{M,0}}{\left(\frac{f_0}{f}\right)^3}$$

$$\varepsilon(f) = 1 + \frac{(\varepsilon_0 - 1)}{\left(\frac{f_0}{f}\right)^3}$$

$$Z_0(f) = \frac{Z_0}{\left(\frac{f_0}{f}\right)^{3+\eta}} \quad (5)$$

where $\rho_{M,0}$, ε_0, Z_0 are, respectively, the electron density, the dielectric permittivity, and the Pauli step barrier at standard pressure. In eq 5, η is a semi-empirical parameter that gauges the strength of the solute–solvent Pauli repulsion. A higher value of the Pauli repulsion parameter η is indicative of a higher Pauli barrier potential $Z_0(f)$ of the medium. The choice of the η parameter should be understood as reflecting the nature of a specified and chemically inert chemical environment. Usual values of the η parameter are within the range η = 3–6[61–63] In this work, a continuum with relative permittivity ε_0 = 2.0165 and a mean electron density $\rho_{M,0}$ = 0.2004 e/Å^3 at standard conditions of pressure has been used as the external medium.

The repulsive step barrier $Z_0(f)$ has been computed using the Pauli repulsion parameter $\eta = 6$. To validate this setting we have compared our results to experimental equations of state of the pressure as a function of volume compression (V/V_1), using as a reference the volume V_1 corresponding to the pressure p = 1 GPa.[64] Good agreement in V/V_1 is seen when comparing to the experimental equations of state available for selected noble gases (Figure 2). The

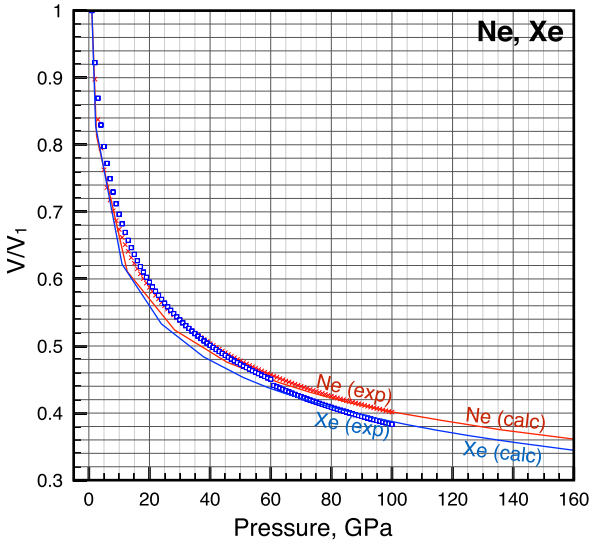

Figure 2. Experimental $T \to 0$ K compression isotherms (available up to 100 GPa[65]) agree with single atom compression modeling of the noble gas elements. One exception is He, for which compression is underestimated (not shown). This deviation is expected, and an explanation as to why can be found in the SI.

best agreement is with the equation of state (isothermal compression without phase changes) for neon. Our model, therefore, most closely resembles a situation in which individual atoms are solvated and compressed by neon.

For each spin state of each atom investigated, we have performed one vacuum reference calculation, and 37 individual compression calculations, throughout which the cavity scaling factor is decreased from f_0 = 1.3 to f = 0.6. This compression suffices to model pressures exceeding 300 GPa for all elements. To calculate the enthalpy of the compressed atoms under constant pressure, we have added to each electronic configuration energy G_{er} an enthalpic term given by pressure, p, times the cavity volume, V_c.

The use of penetrable spherical confinement on a limited set of spherically symmetric atoms (He, Be, Ne, Mg, Ar) has highlighted the drawbacks of using pure density functional theory (DFT) functionals, lacking Hartree–Fock exchange.[66] Inflexibility of the basis set is another well-known issue when compressing atoms.[66–69] Ideally one should optimize the basis set exponents of each element at each stage of compression, which is a massive undertaking. To minimize these concerns, we have used a modified version of Gaussian 09 to perform single-atom and all-electron relativistic DFT compression calculations using the Perdew, Burke, Ernzerhof hybrid-exchange correlation functional PBE0.[70] A Douglas–Kroll–Hess second-order scalar relativistic Hamiltonian[71–75] was used together with the very large and uncontracted atomic natural orbital–relativistic correlation consistent (ANO-RCC) basis set, available for elements 1–96.[76–81] Spin–orbit coupling was found to have negligible effects on atomic properties when calculated relative to a vacuum reference, and could safely be excluded in the generation of the main data set. A more detailed description of the computational procedures and their validation can be found in the SI.

■ ELECTRONEGATIVITY

There are many definitions of electronegativity,[82–99] and the concept has a rich history.[100,101] For our extension of electronegativity of the elements to high-pressure regimes, we follow up on our previous efforts[12,14,102] that define electronegativity as the average electron energy, $\bar{\chi}$. $\bar{\chi}$ may be

DOI: 10.1021/jacs.9b02634
J. Am. Chem. Soc. 2019, 141, 10253–10271

calculated using quantum mechanical calculations or be estimated from photoelectron spectroscopy experiments. Here we will look at atoms, but the $\bar{\chi}$ measure can be consistently defined as well for molecules, infinitely extended crystals, or amorphous matter.[102] Throughout this work we will use the words "electronic level" and "orbital" interchangeably. One computationally simple approximation to $\bar{\chi}$ for atoms, which we will use, is the average energy of all occupied atomic orbitals,

$$\bar{\chi} = \frac{\sum_i \varepsilon_i}{n} \tag{6}$$

where ε_i is the energy of the ith occupied atomic orbital and n is the total number of electrons. $\bar{\chi}$ effectively quantifies how strongly an atom "holds on to its electrons".

When defined in the above manner (eq 6), changes in energy of the average electron, $\Delta\bar{\chi}$, maintain a well-defined connection to the total enthalpy change, ΔH, associated with a given transformation,

$$\Delta H = n\Delta\bar{\chi} + \Delta V_{NN} - \Delta E_{ee} + \Delta(pV) \tag{7}$$

where the $\Delta(pV)$ term describes the enthalpy associated with changing the pressure or volume of the system, ΔV_{NN} is the change in the underlying nuclear−nuclear repulsion energy (= 0 for single-atom processes, such as ionization, electron attachment, or compression of an atom), and where ΔE_{ee} quantifies changes of all manners in which electrons interact with each other (note that in previous publications we referred to $-\Delta E_{ee}$ as $\Delta\omega$). With the exception of ΔE_{ee}, which can be obtained indirectly, all terms of eq 7 can be either calculated, or experimentally estimated. This simple energy partitioning analysis thus relates changes in electronegativity to what actually determines the outcome of most chemical and physical processes—the total enthalpy change.

As previous work has shown,[12,14] the all-electron average $\bar{\chi}$ that we use is best suited for accurate estimates of "electronegativity equalization", or *changes* in $\bar{\chi}$ that occur in chemical transformations, or, here, in physical compression. For more conventional use of the electronegativity concept, for example for comparing numerical values of atoms with one another, a valence-only average is preferable. When the electron binding energy average is taken over only the valence electrons, we arrive at an approximation to Lee Allen's electronegativity scale[11,91,103,104] which agrees well (it correlates linearly) with most other scales of electronegativity. We have previously expanded upon Allen's concept by compiling a table of valence-only electronegativities derived from experimental ground-state ($T \rightarrow 0$ K) photoionization data complemented with quantum mechanical calculations.[102] As we shall see, such a conventional electronegativity scale becomes a valuable reference point when we analyze how the all-electron $\bar{\chi}$ values change under pressure.

In some of our previous work $\bar{\chi}$ values were listed as positive.[102] This was done for discussion's sake when comparing to ionization potentials and other electronegativity scales, which are positive by definition. In this work, $\bar{\chi}$ is defined as an average electron energy relative to vacuum, which is negative in all bound systems under ambient conditions. When interpreting the quantity $\bar{\chi}$ in this work, remember that more electronegative atoms take more negative (or less positive) values of $\bar{\chi}$. *Trends in the electronegativity (high or low) follow the negative of the $\bar{\chi}$ term.*

Before we proceed a warning is justified: Electronegativity arguments can fail. Most chemists know this well. Just as electronegativity is not always capable of predicting the direction of charge transfer or polarity in molecules, for example in CO and BF, or certain trends in bond strength, so it will sometimes fail in extended materials, or under pressure. The advantage of our definition, where electronegativity is the negative of the $\bar{\chi}$ term, is that we connect the concept to the total energy or enthalpy via eq 7. This allows us to reason what occasional failures mean; these may be usually traced to the modulation of multielectron effects captured by the ΔE_{ee} term.

ELECTRONEGATIVITY OF COMPRESSED ATOMS

What do we expect to happen to an atom's electronegativity under pressure? Relative to vacuum, which is the universal reference used in our compression model, compression raises electronic levels.[1,44] Why it does so is easiest seen by a potential energy argument: As a result of compression, some regions of space in which an electron is attracted to its nucleus become unavailable to it (shaded regions in Figure 3). As such,

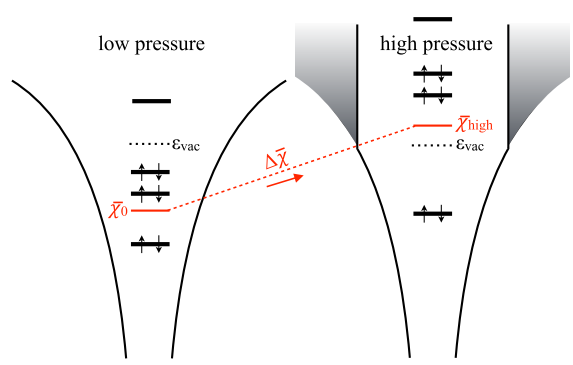

Figure 3. Change in the average electron energy, $\Delta\bar{\chi}$, is used to gauge the effect of pressure on electronegativity. As pressure rises, electronic levels go up, and the electrons become less bound with respect to vacuum, in a manner that is distinctly different for different atoms.

the average electron energy, $\bar{\chi}$, is expected to increase ($\Delta\bar{\chi} > 0$, Figure 3). There is also a kinetic energy argument that explains the raising of electronic levels upon compression: As a result of the reduction in space (by the shaded region if Figure 3), there is an increase of the kinetic energy of the electrons due to the Heisenberg uncertainty and Pauli principles.[105] An increased kinetic energy can translate to less strongly bound electrons and electronic levels of higher energy.

As a reviewer noted, an option available and used in real systems is that the destabilized electrons may enter interstitial lattice sites, forming high-pressure electrides.[44] Here we have not treated the compression of electrons in the absence of an attractive potential.

What is important for chemistry is, of course, the relative electronegativity difference between atoms of different elements at a given pressure. Our first step toward understanding electronegativity as a function of pressure is to calculate the change in the average electron energy, $\Delta\bar{\chi}$ for $p_{1\ atm} \rightarrow p_x$, where $p_x \leq 300$ GPa, i.e., the increase in energy (*decrease* in electronegativity) upon compression relative to the atoms in vacuum. More details can be obtained if in a second step, the $\Delta\bar{\chi}$ set calculated for each atom is offset by the *negative* of an existing ambient pressure scale of electronegativity. We here rely on our recent modification to the

DOI: 10.1021/jacs.9b02634
J. Am. Chem. Soc. 2019, 141, 10253−10271

Allen electronegativity scale, which considers the average valence electron binding energy at 0 K[102] (as opposed to Allen's original full configurational average[91]). Our definition maintains very good agreement with the original scale of Allen and is motivated by the need to extend the original scale to encompass the f-block elements. The Allen electronegativity in turn correlates very well with other electronegativity scales. Thus, any 1 atm scale of electronegativity can, in principle, be used with our $\Delta\bar{\chi}$ data for the purpose of studying how that scale changes with pressure, as long as the units (usually Pauling units, PU) are converted into eV e^{-1}. The conversion factor is 1 PU $\approx$ 6 eV e^{-1}.[104,106] As we shall see, the pressure range that we will investigate ($p \leq 300$ GPa) allows for up to ~3 Pauling units worth of change in electronegativity. The unit of $\bar{\chi}$ that we use (eV e^{-1}) is chosen to highlight the connection between $\bar{\chi}$ and the total energy through eq 7. However, because the physical interpretation of $\bar{\chi}$ can be that of an average electron energy, units of energy (eV) are also acceptable.

The only other attempt at estimating electronegativity of the elements under compression, which we are aware of, is, as we noted, in the manuscript of Dong et al.[43] In that work individual atoms are inserted into an fcc helium lattice, and compression is then modeled using periodic DFT calculations. Electronegativity is there defined from conceptual density function theory,[107] approximated by the Mulliken electronegativity as the average of the ionization potential and the electron affinity. Differences that arise in interpretations and predictions from our work and that of Dong et al. may have several possible origins: (a) the definition of electronegativity (Allen/ours vs Mulliken); (b) the model construction (spherical confinement vs fcc helium); and (c) the level of theory (all-electron relativistic hybrid-exchange-correlation-DFT vs periodic and pseudopotential-based GGA-DFT), as well as other technical details and approximations mentioned by Dong et al.[43] One especially important concern here is the level of theory. Whereas self-interaction errors inherent in a DFT treatment have a rather small effect on calculations of spin pairing in open-shell systems under compression,[108] it can affect individual orbital energies.[109] Such artifacts will influence estimates of the ionization potential, electron affinity, and $\bar{\chi}$ alike. Comparison calculations can be found in the SI.

RESULTS AND DISCUSSION

Our complete data set is rich; in fact, it is too large to exhaustively analyze in this one publication. We will systematically go through the periodic table and bring out and discuss selected examples. The final ground-state configuration and electronegativity predicted at 300 GPa for all atoms can be found last in this Article, in Figure 18.

Elements 1−18. We start with the first 18 elements. The plot in Figure 4 shows how the electrons become progressively more destabilized as the enclosing cavity shrinks and the pressure rises. The average electron energy increases, hence, $\Delta\bar{\chi} > 0$, which is the same as saying the electronegativity decreases. In other words, Figure 4 represents the calculated average electron energy of compressed atoms relative to the corresponding atoms in vacuum, and so begins at $\Delta\bar{\chi} = 0$ eV e^{-1} for $p = 0$ GPa for all elements. Corresponding $\Delta\bar{\chi}$ plots for all other considered elements can be found in the SI.

In Figure 5 we offset the calculated $\Delta\bar{\chi}$ shown in Figure 4 with the negative of an ambient electronegativity scale.[102] For

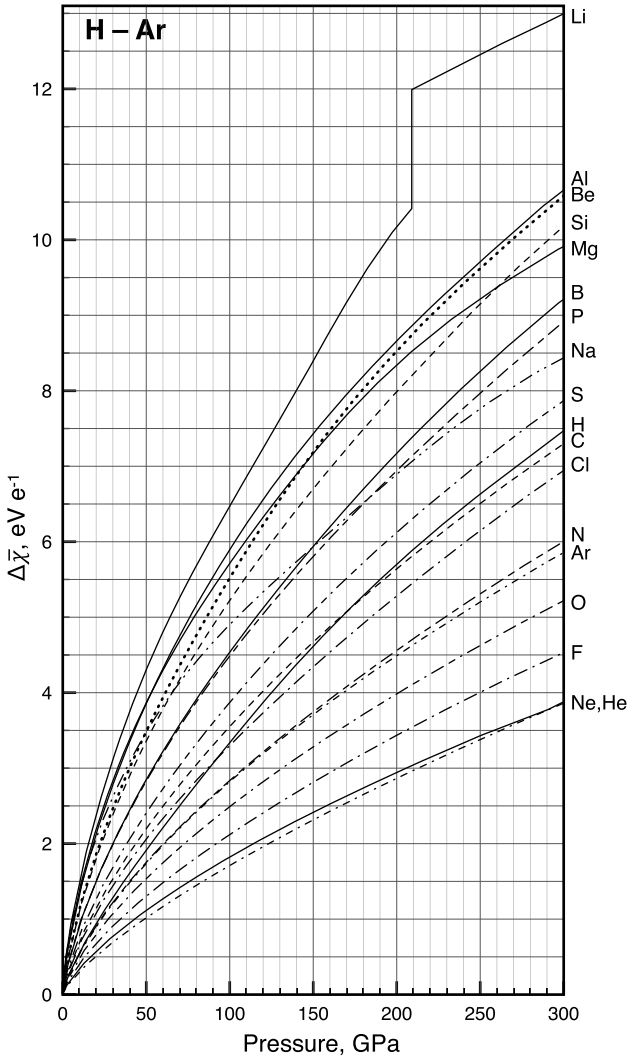

Figure 4. Change in average electron energy, $\bar{\chi}$, upon compression relative to the atom in vacuum. $\Delta\bar{\chi} > 0$ means electron destabilization, i.e., decrease in electronegativity.

example, for carbon the electronegativity is 13.9 eV e^{-1}; Figure 5 shows carbon as the negative of this value at 1 atm. To facilitate a discussion on electronegativity, which here is the negative of $\bar{\chi}$, we plot the y-axis in Figure 5 in reverse. Figure 5 tells us how electronegativity of the different atoms varies with pressure from $p = 0$ to 300 GPa. The zero-value on the y-axis of Figure 5 has no physical significance because under compression the vacuum level is not accessible to the atoms.

Several observations may be made: First, in the pressure range covered, the average electron energy increases (becomes more positive), meaning electronegativity decreases by 4−12 eV e^{-1} (0.7−2 Pauling units). Second, the span of electronegativity for elements 1−18, i.e., the difference between the most and least electronegative, is widened under compression. Electronegative elements, such as He, Ne, F, and O, are affected less by compression than the more electropositive ones.

It is interesting to note the near-zero change in the electronegativity of carbon relative to that of hydrogen under compression. This may be the reason for the invariance of C−H bond lengths with pressure,[1] which undoubtedly has implications for chemistry in deep hydrocarbon repositories.

DOI: 10.1021/jacs.9b02634
J. Am. Chem. Soc. 2019, 141, 10253−10271

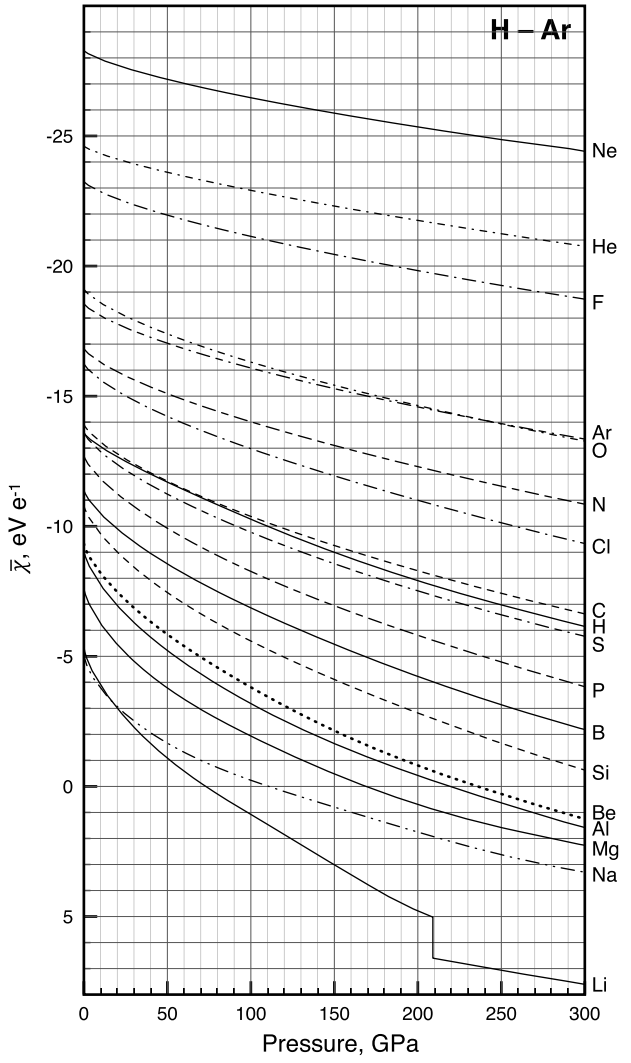

Figure 5. $\bar{\chi}$ as a function of pressure. The *y*-scale is "reversed" so as to facilitate the comparison of electronegativities. More electronegative elements bind their electrons more strongly and are found further up in the figure.

Except for a notable shift in Li and Na, there are no crossings in electronegativity predicted among these first elements below 300 GPa. For Li and Na, these elements start out with very similar electronegativities at 1 atm, where they differ by only 0.3 eV e^{-1}, but where Li is the more electronegative atom.

At a pressure of 300 GPa this difference has increased to 3.6 eV e^{-1}, making Li clearly the more electropositive element of the two by a sizable margin. This is at odds with predictions by Dong et al., who find with their way of estimating electronegativity that Na is the most electropositive element under high compression.[43] There is a distinct kink in the Li curves in Figures 4 and 5 at 210 GPa. We will explain this discontinuity when we turn next to elements in groups 1 and 2.

Alkali Metals. Lithium deserves further comment, because it is the lightest element to exemplify an important physical consequence of compression, namely an actual change in the ground-state electronic configurations of the atom. Our model predicts that lithium undergoes a change in its ground-state electronic configuration, $1s^2 2s^1 \rightarrow 1s^2 2p^1$, at ~210 GPa (Figure 6). The stronger destabilization of a Li 2s electron relative to a 2p under compression has been seen in earlier work.[44,110−116]

Of course, the transition value of 210 GPa in lithium refers to the single atom, isolated in a non-reactive neon-like medium. In lithium metal, or in some alloy of lithium, interactions of orbitals in neighboring atoms would modify the picture. In a study by one of us with Maosheng Miao, we studied the Li atom transition in another way, by putting a Li atom into an fcc He lattice as a compression medium.[44] The corresponding transition takes place at 100 GPa in that model. The different results between the models is in part due to differences in the level of DFT theory (see the SI).

The general phenomenon of pressure modulating the energy of orbitals, and frontier orbitals in particular, is very important. It can be rationalized from the different spatial extents of orbitals. All electronic atomic levels increase in energy with compression, but there is an important, determinative difference between orbitals of different orbital angular momentum quantum number, l, for the same principal quantum number, n. As a plot of hydrogenic orbitals readily reveals, the number of radial nodes, $(l - 1)$, matters a lot. The more radial nodes an hydrogenic orbital has (4s > 4p > 4d > 4f), the further out from the nucleus is its peak density, and at some distance beyond that peak density—this is the region of space where the effects of pressure are felt the most—the density falls off in the order indicated. To put it another way, an *n*s orbital's density spreads further out from the nucleus than that of an *n*p orbital, because the *n*s orbital has to stay orthogonal to more core orbitals than does an *n*p. The farther out from the nucleus the resulting electron density is, the more it is affected by external pressure.[44] Note that this explanation is a first approximation based on hydrogenic orbitals. The frontier orbitals of many-electron atoms can behave differently.[117]

Transition pressures between competing electronic configurations are defined as a point of equal enthalpy. Note that whereas the $\Delta\bar{\chi}$ plot of Li contains a distinct kink (Figures 4−6), the total enthalpy ($H = E + pV$) of the system increases smoothly as a function of pressure over the electronic transition (Figure 6). The total energy (E) also increases smoothly over the transition, but then as a function of the cavity radius and not pressure (not shown). The kink in the lithium curve in Figures 4−6 comes about because of a contraction of the electronic wave function at the 2s→2p transition. For these transitions the state before the transition corresponds to a larger cavity radius, and the state after the transition corresponds to a smaller radius. In other words, isobaric transitions typically correspond simultaneously to two different cavity radii. The example for lithium in Figure 6, shows how, to ascertain the precise transition pressure, we have extrapolated from explicit calculations near the transition. In general, the intersection points have been determined by extrapolation to less than 10 meV difference in enthalpy. For most atoms, this translates to an uncertainty in the transition pressure below 5 GPa. More details on how the transition pressures are determined will be outlined when we discuss Ca.

To understand the driving force for the increase in the energy of electronic levels ($\Delta\bar{\chi} > 0$) in a complementary way, we can apply eq 7. If we consider the crossing point between two configurations, then ΔH between them is equal to zero. Thus, at this point of crossing we must have $n\Delta\bar{\chi} = \Delta E_{ee} - p\Delta V$. In the typical case of a pressure-induced configurational change, the variation of the total electron energy, $n\Delta\bar{\chi}$, is

DOI: 10.1021/jacs.9b02634
J. Am. Chem. Soc. 2019, 141, 10253−10271

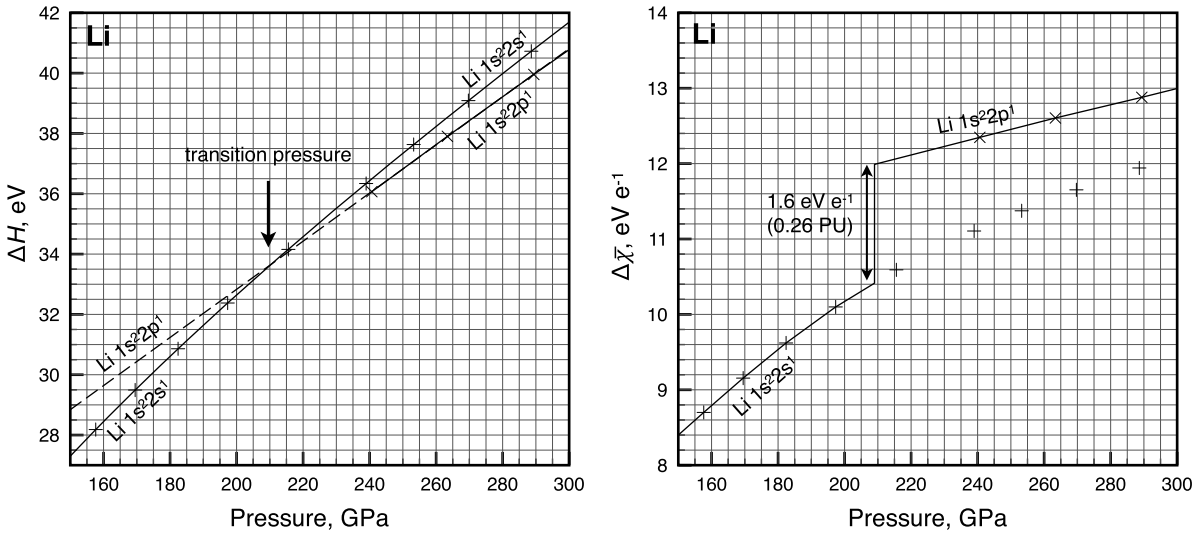

Figure 6. Left: A rare s→p one-electron transition is predicted in lithium at ∼210 GPa. The transition pressure is identified though extrapolation (dashed line) from explicit calculations (crosses and plusses) of the two competing electronic configurations. Right: Final data set (black line) shows the decrease in electronegativity ($\Delta\bar{\chi} > 0$ means electron destabilization) of lithium relative to that at p = 1 atm.

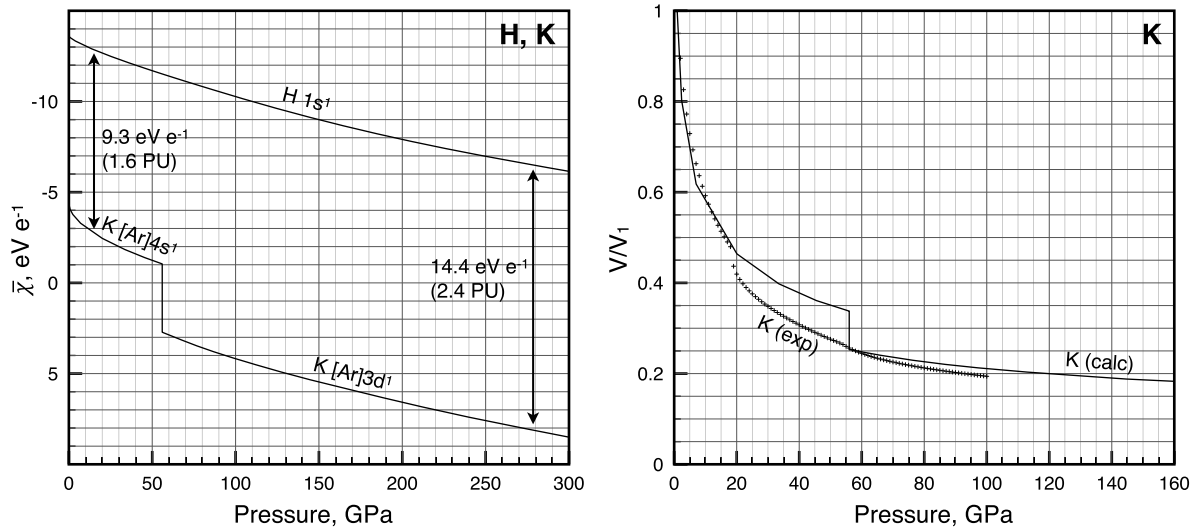

Figure 7. Left: The potassium atom is predicted to undergo a one-electron s→d transition at ∼56 GPa. This transition points to a different reactivity and structural chemistry of potassium at higher pressure. The evolution of the electronegativity of hydrogen, also shown for comparison, is smooth. More negative values mean more electronegative, and the y-axis is reversed so as to facilitate the analysis. As pressure increases in this region, K−H interactions are predicted to become more polar and directional in nature. Right: Experimental equation of state[65] for elemental potassium compared to the atomic compression model.

positive. The variation of the electron−electron term, ΔE_{ee}, is also positive. As the volume decreases, the corresponding $p\Delta V$ term is negative.

In other words, pressure-induced configurational changes occur concomitant with increases in electron interactions. Because ΔE_{ee} is often the largest negative term in the energy partitioning shown as eq 7, one can take the viewpoint that the increasing electron interactions are, in fact, enabling such configurational transitions. An analogy with charge transfer reactions, where this behavior is typical,[14] is meaningful because in compression of atoms electrons are transferred into ever smaller volumes. We have identified only a few exceptions to this rule, in Tb, Dy, and Ho, described later. The magnitude of the $p\Delta V$ term is typically smaller than the other terms, but is significant as it can lower transition pressures by several tens of GPa. We have not analyzed the importance of the $p\Delta V$ term in detail.

The s→p one-electron transformation in Li is, as far as we can tell, the only one of its kind in the periodic table in the pressure range studied. It causes a rather small (1.6 eV e^{-1}) but sharp increase in $\Delta\bar{\chi}$ at 210 GPa, i.e., a decrease in electronegativity. Lithium appears to be the only atom in the periodic table that by itself (without chemical interactions) is capable of transforming into a p-block element under compression below 500 GPa. Beryllium, sodium, and calcium might be the other examples, but at degrees of compression far above where our model have been validated.

To introduce a much more prevalent (and long known, suggested by Fermi[118]) kind of electronic restructuring, we look next at potassium. Compression has a dramatic consequence for the potassium ground state: 3d levels,

DOI: 10.1021/jacs.9b02634
J. Am. Chem. Soc. 2019, 141, 10253−10271

formally unoccupied at 1 atm, drop below the 4s valence orbital under pressure, resulting in an $[Ar]4s^1 \rightarrow [Ar]3d^1$ one-electron transition (Figure 7, left). In our model for potassium (as an isolated, compressed atom) the transition is predicted to occur at ∼56 GPa. The experimental information, on metallic K, shows a sharp discontinuity in the equation of state at ∼20 GPa. The attached specific volume drop is similar in magnitude to what we predict for the isolated atom at ∼56 GPa (Figure 7, right). The reader will notice that there is a region of pressure 20−56 GPa where the experimental and calculated K equations of state differ much. The problem is not in our calculation of the $p-V$ relationship (see pretty good agreement in the right panel in Figure 7), but in the prediction of the pressure at which the s→d transition takes place. The calculation is for an atom, the experiment is for bulk K metal. The discrepancy is not surprising. The helium compression model has this transition occurring at a lower pressure, ∼20 GPa.[44]

$ns \rightarrow (n-1)$d transitions, such as that calculated and observed for potassium, occur for many other elements, as we shall see. A chemical consequence of Figure 7, for example, is that it clearly suggests that the reactivity of potassium with respect to hydrogen will increase with pressure; not only does the K atom transform into a d-element, but its electronegativity is also drastically decreased with respect to that of hydrogen. This is in accord with the predicted stability of different potassium polyhydride phases, such as KH_6, under pressure.[119−121]

We suspect that configurational transitions can be used to explain, or predict, both changing reactivity and directionality of chemical bonds in alloys of heavier alkali and alkaline earth metals, and other atoms, under pressure. A higher reactivity and polarity would be anticipated in cases where the difference in electronegativity between constituent atoms increases upon compression. Conversely, decreases in electronegativity differences under pressure predict lower reactivity and a lessened polarity between atoms.

By directionality of chemical bonds, we refer to arrangements of surrounding atoms/ions around a reference atom that may be traced to the non-spherical orbital topology of the participating atoms. Oxidation states play a role here. For example, in KF, potassium may be best considered as K^+. In such a case, the existence of a d^1 configuration of the K atom under pressure is likely less important or irrelevant for guiding structure. In other words, directionality of bonding is unlikely to be exhibited in the ionic limit where structures are composed of oppositely charged, effectively spherical, ions. However, if we consider a metal alloy in which potassium is *not* oxidized (or not fully oxidized), we would argue that the orbital topology around the K atom will be more symmetric under normal conditions (in the s^1 configuration) and less symmetric under high pressure (d^1 configuration). Pressure-induced phase changes occurring in such alloys can be interpreted as being due to increased directionality in bonding, concurrent with an s→d valence transition of the potassium atom.

The same kind of $ns \rightarrow (n-1)$d transitions as are known in potassium are also calculated for the heavier group 1 atoms Rb, Cs, and Fr. These atoms have similar electronegativity at 1 atm.[102] However, as we already saw for Li, small differences in electronegativity at 1 atm are of little consequence to any comparison under the pressures discussed here, where relative changes between atoms tend to be large, and on the order of several eV e^{-1}.

Figure 8 shows the electronegativity evolution of all of the alkali elements on the same scale. *More negative values mean more strongly bound electrons and more electronegative atoms in the usual sense of the word.* Thus, the interesting prediction here is that a reordering occurs. The common 1 atm ordering of electronegativity, Cs < Fr < Rb < K < Na < Li, is predicted to change into K < Rb < Li < Cs < Fr < Na at 300 GPa. We can trace the inversion in electronegativity of the heavier alkalis to the magnitudes of their $\Delta\bar{\chi}$ upon $ns \rightarrow (n-1)$d transition (in eV e^{-1}): K(+3.8) > Rb (+2.2) > Cs(+1.7) > Fr (+1.4). Note that Na, as expected, does not undergo an s→d transition. The calculated transition pressures are strikingly similar for all, ∼55 GPa, except Cs, which is predicted to transform at ∼25 GPa.

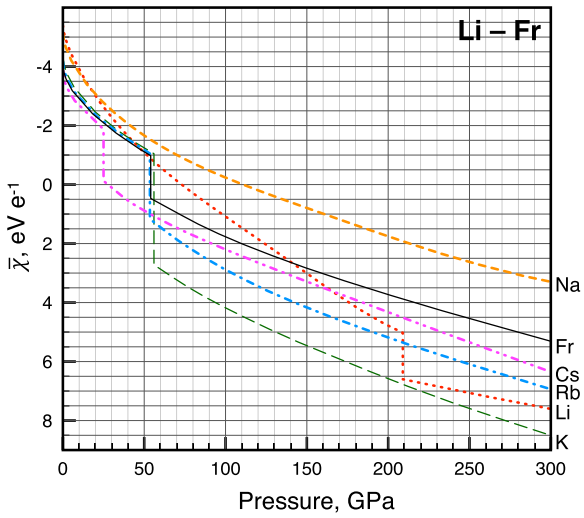

Figure 8. Electronegativity of the alkali metals undergoes a dramatic reordering under compression. The reordering is caused by a decreasing s−d splitting down the periodic table and an absence of any configurational transition in Na in this pressure range. Increasing average electron energy, $\Delta\bar{\chi}$, relative to the atom in vacuum is here offset by electronegativity tabulated under normal pressure conditions. As in earlier figures, the *y*-scale is reversed so as to facilitate comparison of electronegativities, where up means more electronegative.

There are implications of the ordering predicted for the direction of ionicity in compressed alloys of the alkali metals. The changes could be quite drastic in the observable pressure range. The range of electronegativity differences between the alkali metals changes from 1.5 eV e^{-1} at 1 atm to ∼5 eV e^{-1} at 300 GPa. These results are, for example, in good agreement with predictions of high pressure $CsLi_n$ intermetallics.[122] In such phases, Cs (now a d-block metal) can take on a negative charge beyond −1.

A reviewer has noted an important point: Because the application of pressure destabilizes lower angular momentum orbitals the effect we discuss could manifest itself not only in valence level switches, for example, as $ns \rightarrow (n-1)$d transitions, but also operate on sub-valence, or near-core levels. So $(n-1)$p levels, usually viewed as core ones, may come above *ns* levels. This appears to happen in Cs, for instance, in the work of Maosheng Miao.[122,123] Whereas we do not discuss reordering of occupied levels here, all valence, sub-valence, and core levels are included in our calculations of $\Delta\bar{\chi}$.

DOI: 10.1021/jacs.9b02634
J. Am. Chem. Soc. 2019, 141, 10253−10271

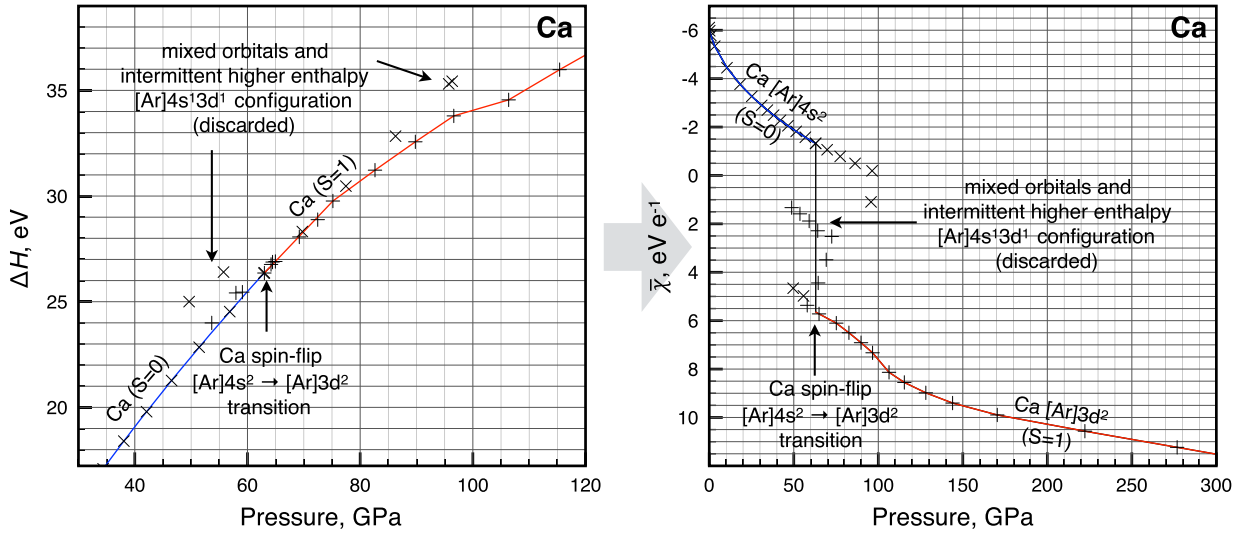

Figure 9. Compression of the calcium atom exemplifies how our data have been processed. Left: The total enthalpy of an atom relative to its vacuum reference is shown for explicit calculations on singlet (crosses) and triplet (pluses) states of the Ca atom as a function of pressure. Intermittent higher energy configurations can be omitted, leading to the final data set, which is indicated as a solid line (blue for singlet and red for the triplet state). Ca is predicted to undergo a two-electron s→d transition at ~63 GPa. Right: The electronic transition causes a sharp decrease in the average valence electron energy, which coincides with a decrease in the spatial extent of the atomic wave function (not shown). The *y*-scale is reversed in the right figure so as to facilitate comparison of electronegativities, where up here means more electronegative.

Alkaline Earths. Beryllium and magnesium behave normally; the evolution of their electronegativities with pressure was already shown in Figure 5. The s→p transitions for these elements (see discussion for Li) might occur at pressures way outside the range examined in this work. Beginning with calcium, the complexity observed increases, and this will give us an opportunity to explain some more details of our analysis. As was the case for K, the configuration switch in Ca is 4s→3d. However, in contrast to the previous examples of Li and K, in Ca *two* electrons change character, and there is an accompanying change of spin state from singlet to triplet: $[Ar]4s^2$ ($S = 0$) → $[Ar]3d^2$ ($S = 1$). *For all elements (atoms) in which spin-crossover is suspected, we have subjected each potential spin state to the compression procedure.* By plotting the total enthalpy of competing states versus the pressure, we can identify the crossing point at which the spin of the ground state changes (at left in Figure 9).

In many cases, as for Ca, the transition in the orbital occupations of the electrons (for example, s→d) occurs in several competing spin states. For example, for Ca, the 4s→3d transition is calculated to occur at 87 GPa on the singlet surface (not shown). The transition occurs earlier, at 63 GPa, due to a crossing with the triplet surface (Figure 9). The difference between the two spin states is that on the singlet surface the resulting $[Ar]3d^2$ configuration lies higher in energy due to the two 3d electrons being spin paired. The spin-flip itself has important consequences for the total energy, but has only a small influence on the drop in electronegativity that follows the change in orbital occupations of the electrons.

Because the calculations we perform do not specify spatial symmetry, and new guesses for the orbitals and their occupancy are made for each cavity volume, occasional higher energy solutions can appear. By always following the lowest energy state attributed to a given pressure, these higher energy configurations can be discarded, and we can then investigate how different atomic properties, such as electronegativity, change with pressure (at right in Figure 9).

Looking at all the alkaline earths in Figure 10, we see, as for the alkali metals, a complete reversal of the order of

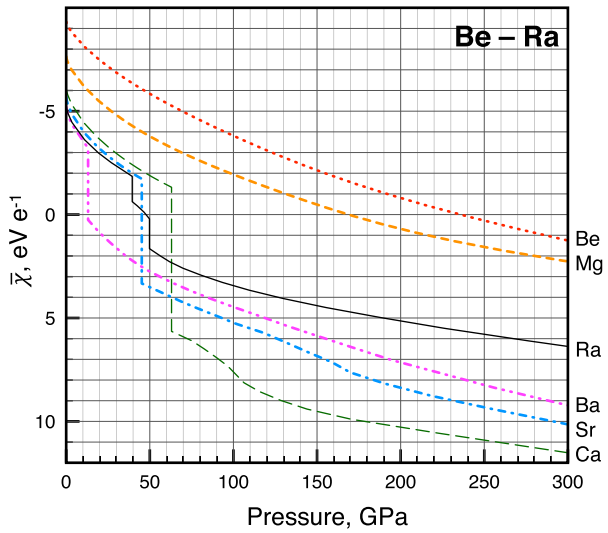

Figure 10. Compression of the alkaline earths. The increasing average electron energy, $\Delta\bar{\chi}$, relative to the atom in vacuum is here offset by electronegativity tabulated under normal pressure conditions. The *y*-scale is reversed so as to facilitate comparison of electronegativities, where, as in Figure 9, up means more electronegative.

electronegativity of the heavier elements. Again, whether we start out with the Allen scale, the Pauling scale, or with our more recent revision of electronegativity is of little consequence for our predictions, for the energy differences between the scales and the atoms at ambient conditions are much smaller than those under compression. For example, the difference in electronegativity between Ra and Ba is 0.3 eV e^{-1} at ambient conditions, but grows by an order of magnitude to 2.8 eV e^{-1} at 300 GPa (Figure 10).

DOI: 10.1021/jacs.9b02634
J. Am. Chem. Soc. 2019, 141, 10253−10271

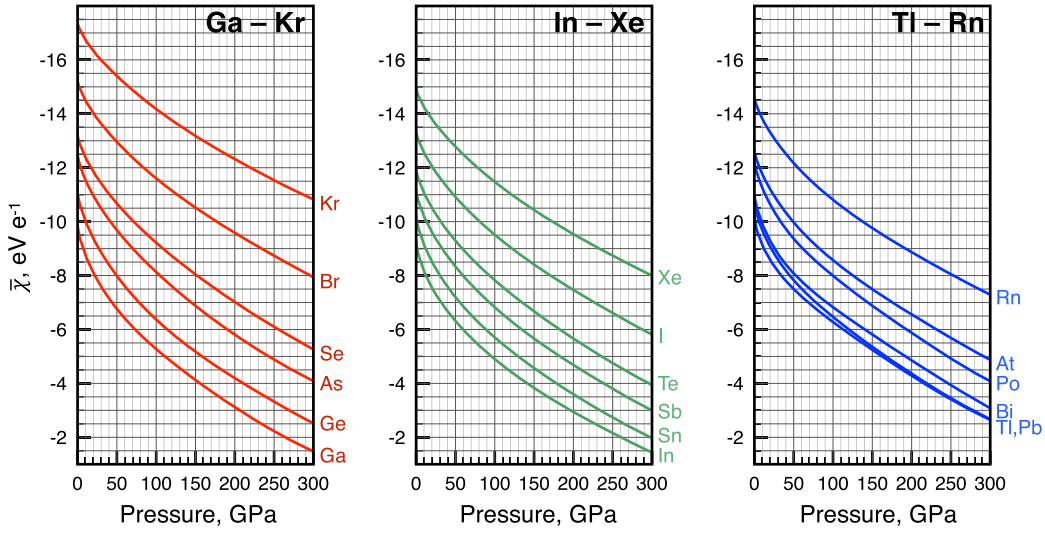

Figure 11. Changes in average electron energy, $\Delta\bar{\chi}$, relative to the atoms in vacuum offset by electronegativity tabulated at 1 atm. $\bar{\chi}$ is shown as a function of pressure for the heavier main group atoms, Ga−Kr (red), In−Xe (green), and Tl−Rn (blue). The *y*-scale is reversed so as to facilitate comparison of electronegativities, where, as in previous figures, up means more electronegative.

The pressures at which $ns \rightarrow (n-1)$d transitions occur in the heavy alkaline earths are more spread out compared to the alkali metal series. Ba, the atom with the lowest electronegativity at 1 atm, transitions into an $[Xe]5d^2$ configuration at ∼13 GPa. Ra transitions first into an $[Rn]7s^16d^1$ open-shell singlet at ∼40 GPa and onward to a triplet $[Rn]6d^2$ configuration at ∼50 GPa. Sr transition into its corresponding d^2 configuration at ∼45 GPa. Ca, the atom with the largest s-d gap at 1 atm, transitions last at ∼63 GPa.

We stress that the numbers in Figure 10, based on isolated atom calculations, should not be taken as precise predictions of solid-state phase transitions. Rather, as with electronegativity in molecular chemistry at ambient conditions, we expect that it is the relative ordering of these numbers that will be of predictive use. In either covalently (few) or ionically bonded compounds of the alkaline earth, or in the corresponding elemental solids, the question of the spin states of a pressurized neutral atom is not directly relevant.

To relate our results to real compressed solids we first looked at the experimental phase transitions in the alkaline earth metals. The phase diagram of single elements can be complex. Sr, for example, exhibits phase transitions at 4, 26, 35, and 46 GPa at ambient temperature.[124] To enable a comparison with our data, we limit ourselves to Ca, Sr, and Ba, which all have one thing in common: an intermittent low-pressure bcc phase, which transforms into one or another complex phase at ∼32, ∼26, and ∼6 GPa, for Ca, Sr, and Ba, respectively.[124] Because these experimental data are for ambient temperature and have not been corrected for hysteresis, an absolute comparison is not strictly possible. However, we note that the relative trend fits with our calculated s→d transitions.

Magnetism. We note that our calculations sometimes predict singlet ns^2 and sometimes a triplet nd^2 configuration of the high-pressure alkaline earth atoms. Thus, we have answered here a question posed earlier—can magnetism arise under pressure? It can for atoms, but there is not necessarily a direct implication here for extended structures. Nevertheless, pressure has been predicted to induce ferromagnetism in certain phases of alkali metals,[125,126] and pressure is experimentally known to induce magnetism in various iron alloys[127,128] Magnetic order for Fe under pressure is controversial,[129] as is that of O_2.[130,131] As we will see when we discuss the atoms of the d-block, magnetism in atoms is not always predicted to increase upon compression. In several instances, the reverse is expected.

Main Group Elements 31−36, 49−54, and 81−86. Compared to most other constituents of the periodic table, the relative differences between the heavier atoms of the "main" groups (alternatively called p-block elements), Ga−Kr, In−Xe, and Tl−Rn, are largely unaffected by compression. All p-block atoms retain their 1 atm ground-state electronic configuration up to 300 GPa. Figure 11 shows the evolution of electronegativity for p-rows 4, 5, and 6. Ga−Kr maintains a relatively large spread in electronegativities of ∼9 eV across the investigated pressure range. Similarly, the In−Xe and Tl−Rn series maintain their spreads of ∼6 and ∼4 eV, respectively. These results mean that, as a rule of thumb, when comparing electronegativities within p-blocks, the pressure variable does not destroy the chemical intuition earned at 1 atm—an increase in electronegativity as one moves from group 13 to 18. Nevertheless, differences in reactivity are predicted. For example, whereas the electronegativity difference between Kr and O is small under ambient conditions, a 1.2 eV e^{-1} difference at 1 atm is increased to 2.6 eV e^{-1} at 300 GPa. This is in qualitative accord with a predicted stability of KrO near the latter pressure.[132]

It should be noted that whereas pressure induces little relative change of electronegativity between atoms of the main groups, most such atoms develop their electronegativities at markedly different rates compared to atoms in other blocks. Changes in electronegativity between atoms allow one to make interesting predictions on the nature of polarity, and reactivity in various compressed binary alloys. For example, whereas the 7.3 eV e^{-1} difference between Mg, and Xe is insufficient to cause a reduction of Xe at 1 atm, the difference grows to 10.3 eV e^{-1} at 300 GPa, and stable compounds with negatively charged Xe have been predicted at this pressure.[133] The difference of 10 eV e^{-1} exceeds that between Xe and F under

DOI: 10.1021/jacs.9b02634
J. Am. Chem. Soc. 2019, 141, 10253−10271

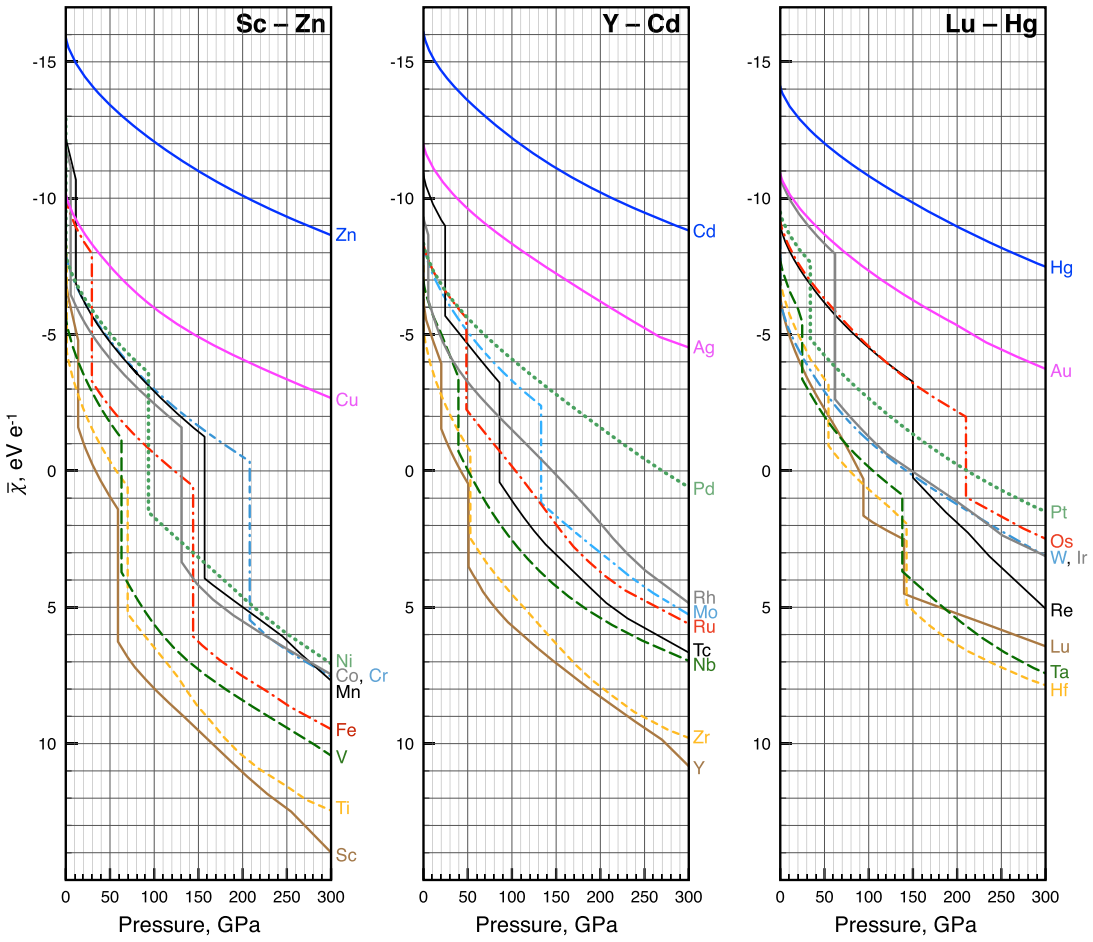

Figure 12. Compression of row 4 d-block atoms Sc−Zn (left), row 5 d-block elements Y−Cd (middle), and row 6 d-block elements Lu−Hg (right). Increasing average electron energy, $\Delta\bar{\chi}$, relative to the atom in vacuum, is here offset by electronegativity tabulated under normal pressure conditions. As earlier, the *y*-scale is reversed in all figures so as to facilitate comparison of electronegativities, where up means more electronegative. All vertical lines in these figures correspond to one-electron s→d transitions starting from the 1 atm ground-state atom configuration at p = 0 GPa, except for Re, Os, and Ir where two-electron transitions are indicated. Hund's rule is followed in all transitions, so that the value of $\langle S\rangle$ is maximized for any given configuration. Note that our calculations incorrectly predict the ground-state configuration of Zr to be $5s^14d^3$ instead of $5s^24d^2$ at 1 atm, and that of W to be $6s^15d^5$ instead of $6s^25d^4$ at 1 atm. Experimentally the competing configurations are near in energy: 0.6, and 0.37 eV at 0 K for Zr, and W, respectively, and a s→d transition can be assumed to occur at mild compression. The $6s^15d^5$ configuration of W is predicted to persist up to 300 GPa.

normal conditions (8.4 eV e^{-1}), where electrons flow the other way.

Transition Metals and Hund's Rule under Compression. The data for all transition metal atoms, or the d-block, is summarized in Figure 12. With the d-block, we return to the familiar trend established for the alkali and alkaline earth atoms: ground-state configurations transform s→d with increasing pressure. With even more possibilities for transitions between configurations and spin states, it is pertinent to first address possible rules for these transitions.

Hund's first rule (or simply, Hund's rule) describes the common tendency of atomic and molecular systems with degenerate levels to favor high-spin over low spin ground states.[134] The mechanism behind this rule is the minimization of electron Coulomb repulsion through exchange correlation of like-spin electrons. Hund's rule violations are rare under ambient conditions, but they do exist. Kollmar and Staemmler have attributed some violations to spin polarization effects,[135] and Hrovat and Borden have explained how, in molecules, Hund's rule violations tend to occur in diradical systems with disjoint frontier orbitals.[136] Some examples of Hund's rule violations under ambient conditions are in dinitrogen complexes of chromium,[137] in certain quantum dots,[138] and in graphene nanoflakes.[139]

Hund's rule is followed in the investigated pressure range insofar that for all considered transitions, the value of $\langle S\rangle$ is maximized for any given configuration. For example, for scandium (Figure 12) the ground-state configuration and spin-state changes as $[Ar]4s^23d^1$ (S = 1/2) → $[Ar]4s^13d^2$ (S = 1.5) → $[Ar]3d^3$ (S = 1.5), when pressure increases from 1 atm to 300 GPa. Note that there are several examples where the maximum spin of the final configuration is smaller than the ground state at 1 atm, i.e. where magnetism is predicted to decrease. For example, the transition in Cr is $[Ar]4s^13d^5$ (S = 3.0) → $[Ar]3d^6$ (S = 2.0). Because $[Ar]3d^6$ is the predicted ground-state configuration of Cr under compression, while spin $\langle S\rangle$ = 2 is the maximum possible in the $[Ar]3d^6$ configuration, examples of such spin reduction are *not* violations of Hund's rule. A reduction in spin following compression to 300 GPa is predicted in all d-block atoms for which the valence d-shell occupation n at 1 atm is d^n ($4 \le n \le 8$). The one exception is Nb, for which $\langle S\rangle$ does not change

DOI: 10.1021/jacs.9b02634
J. Am. Chem. Soc. 2019, 141, 10253−10271

upon compression. Nb has a $[Kr]5s^14d^4$ ground state, which, as we shall see, changes into $[Kr]4d^5$ under compression.

As far as we can tell, Hund's rule is never violated for single atoms in the considered pressure range. However, as the example of Cr shows, Hund's rule is still subservient to the *aufbau* principle, which, as Connerade and co-workers predicted,[42] indeed appears strengthened under pressure. As we shall see later, there are a couple of possible exceptions to this order identified among the f-block elements. Finally, we note that the Madelung energy ordering rule (that orbitals with a lower $n + l$ value are filled before orbitals with a higher $n + l$ value) is not predictive for atoms under compression.

Having established the qualitative rules that govern the majority of the predicted transitions, we return to electronegativity. One especially striking observation, seen when comparing Figure 12 with Figures 8 and 10, is that several d-block atoms, while falling in electronegativity with compression, are predicted to become *less* electronegative compared to most of the atoms of group 1 and 2. For example, *Sc and Ti are predicted to be less electronegative than all group 1 and 2 elements at sufficient compression.*

We also note that several atoms, Ti, V, Mn, Co, Ni, Zr, and W, are predicted to undergo s→d transitions under *very* mild compression. Because $ns \rightarrow (n-1)d$ transitions are synonymous with a marked decrease in electronegativity, such early transitions may have implications for the chemistry of these atoms also under ambient conditions. The formation of chemical compounds can be viewed as imposing a "chemical pressure" on the atoms.[140,141] With this in mind, our results imply that from a practical point of view tabulated atomic electronegativities of these elements (including ones calculated by us)[102] may be overestimated at 1 atm.

Of course, numerous relative changes occur within this subset of atoms and with respect to atoms in the rest of the periodic table. The ability to read out electronegativity as a function of pressure allows for deepened insight into greatly varying transition metal chemistry under compression. For example, the difference in electronegativity between Fe and Xe is increased significantly, from 4.8 eV e^{-1} at 1 atm to 17.5 eV e^{-1} at 300 GPa (Figures 11 and 12). Both calculation and experiment have suggested that Fe/Ni−Xe alloys in Earth's core could be an explanation for the "missing Xe paradox".[142,143] Our data predict the stability of numerous other transition-metal noble gas alloys under pressure. More specific predictions will be discussed in future publications.

A final general point is made by these calculations; the relative rise in energy with pressure of *n*s and $(n-1)$d orbitals ensures that by 300 GPa almost all such transitions that can occur in fact will. The single exception appears to be W, which is predicted to maintain a $6s^15d^5$ ground state beyond 300 GPa. The avoidance of a $5d^6$ configuration can be explained by the non-existence of a corresponding excited state in W below ionization under ambient conditions. We also repeat our caveat: what happens in a compressed atom is not an exact guide, or may have different consequences for an elemental solid or a molecule containing that atom.

The f-Block. The elements of the f-block are difficult to treat computationally, and with that in mind a further comment on our level of theory is in order. In our previous work, outlining the valence-only definition of electronegativity,[102] we relied on the General Multi-Configurational Quasi-Degenerate Perturbation Theory (GMC-QDPT) method[144] to obtain relevant ionization potentials for the valence levels where experiments were missing. Because we desire a correlated treatment of all electrons, not only of a limited valence set, comparable levels of multireference methodology are simply intractable for our purposes here. The DFT treatment that we have used in this work is by no means ideal for treating f-block atoms, but we nonetheless believe it provides useful qualitative information as to what can be expected from actinide and lanthanides atoms under high compression. The reasons for this are as follows:

We know from previous work[10] that the DFT method that we are using (full potential and relativistic PBE0) readily converges to the ground-state electronic configuration for atoms 1−96 at 1 atm, with few exceptions across the periodic table. The only identified exceptions are Zr, Fe, V, W, and Np, and in those cases the SCF procedure still converges to the lowest energy configuration allowed by the KS-Hamiltonian used.

There is little reason to suspect that the method used would perform any better or worse when combined with the XP-PCM compression model, compared to when it is applied for calculations in vacuum. In this work, Np, along with Th and U, could not be sufficiently converged over the entire 300 GPa range, and have for this reason been omitted.

Furthermore, because all properties are calculated relative to a vacuum reference, error cancellation plays an important role. We are primarily concerned with $\Delta\bar{\chi}$, which is a relative measure that has been previously shown to be largely insensitive to the level of theory.[14] Subtleties such as spin−orbit coupling also show negligible effects on our results (see the SI). The energy differences between competing configurations are typically significant except near the transition pressure (cf. Figure 9), and we therefore expect predictions of preferred configurations at high compression to be at least qualitatively meaningful.

The general trend observed across the f-block is similar to the pressure induced $ns \rightarrow (n-1)d$ transitions prevalent in the s- and d-blocks. However, $(n-1)d \rightarrow (n-2)f$ transitions are additionally predicted to occur for some elements in the investigated pressure range. The argument for why this can be expected should now be familiar: $(n-2)f$ orbitals are physically smaller than $(n-1)d$ orbitals for a given atom. Exchange repulsion due to interactions with the surrounding environment is the primary means by which microscopic pressure is mediated, meaning that at sufficient compression f-level occupation can become energetically favored. *Given how important the f-orbital occupation is to the often-desirable physical properties of the lanthanides (such as luminescence, magnetism, and redox character) the effect of pressure on such properties may have significant consequences.*

Cerium is the first atom with an f-occupation under ambient conditions and will serve to illustrate a relatively common pattern of behavior of f-block atoms under compression: close proximity and crossing of multiple electronic configurations and spin states. Figure 13 traces how the average binding energy and the electronic configuration of the Ce atom change under pressure and shows two s→d transitions at ∼5 and ∼18 GPa, followed by one d→f transition at higher compression, ∼270 GPa. Corresponding data for the remaining six of the first seven atoms of the lanthanide series (La−Eu) can be found in Figure S9. *One consistent observation that can be made is that magnetism of these f-block atoms continues to increase with pressure.*

DOI: 10.1021/jacs.9b02634
J. Am. Chem. Soc. 2019, 141, 10253−10271

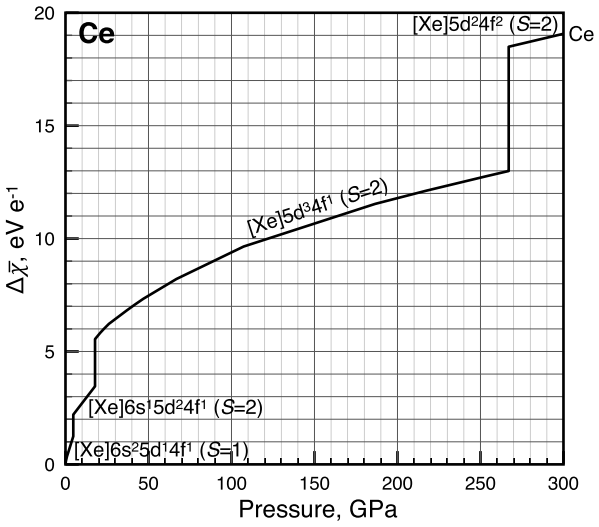

Figure 13. Change in average electron energy, $\Delta\bar{\chi}$, upon compression of Ce relative to the atom in vacuum. $\Delta\bar{\chi} > 0$ means electron destabilization, i.e., decreasing electronegativity. Ce is predicted to exhibit three configurational transitions in the investigated pressure range.

The electronegativity evolution of the first seven atoms of the lanthanide series (La–Eu) are shown at left in Figure 14. The most striking relative changes compared to ambient conditions occurs near 300 GPa, where Ce is predicted to become the least electronegative atom of the entire f-block. The reason for the large decrease predicted near 300 GPa is the configurational transition shown in Figure 13. Ce is unique in showing electronic transitions at such high pressures. The ground-state configurations of most other atoms are predicted to be unchanged near 300 GPa.

We turn next to the seven last elements in the lanthanide series, Gd, Tb, Dy, Ho, Er, Tm, and Yb. The evolution of the ground-state configuration of these atoms can be found in Figures 15 and S11. Out of these, Tb, Dy, and Ho are special,

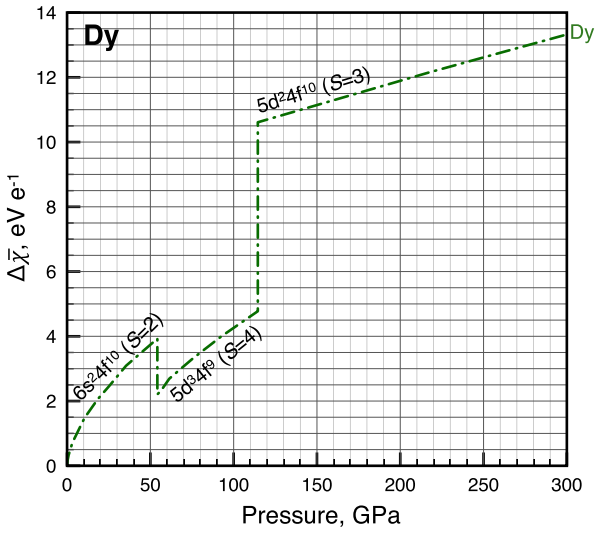

Figure 15. Change in average electron energy, $\Delta\bar{\chi}$, upon compression of Dy relative to the atom in vacuum. $\Delta\bar{\chi} > 0$ means electron destabilization, i.e., decreasing electronegativity. Dy is predicted to exhibit a rare (unique to only Tb, Dy, and Ho) 4f→5d one-electron and 6s→5d two-electron transition at ∼54 GPa. A stabilization of electrons, or increase in electronegativity, is predicted in a span of ∼15 GPa after the transition.

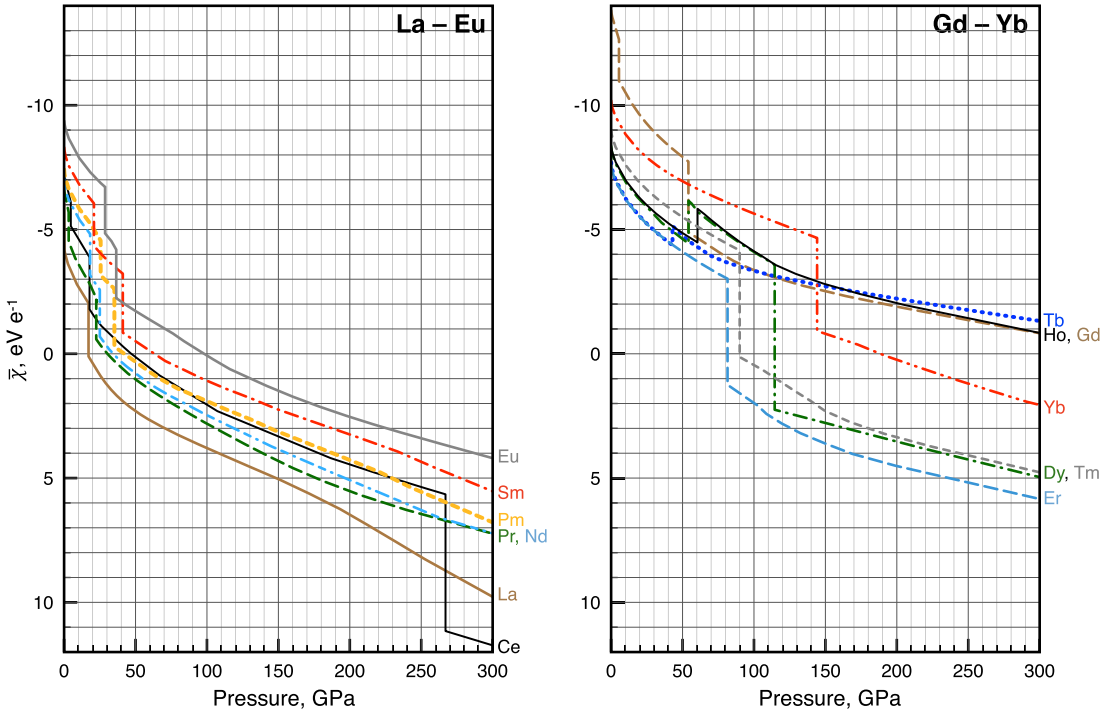

Figure 14. Compression of the lanthanides up to 300 GPa. Increasing average electron energy, $\Delta\bar{\chi}$, relative to the atom in vacuum is here offset by electronegativity tabulated under normal pressure conditions. As earlier, the y-scale is reversed so as to facilitate comparison of electronegativities, where up means more electronegative. Vertical jumps correspond to the electronic configurational transitions indicated in Figures 13 and S9 (for La–Eu) and Figures 15 and S11 (for Gd–Yb).

DOI: 10.1021/jacs.9b02634
J. Am. Chem. Soc. 2019, 141, 10253−10271

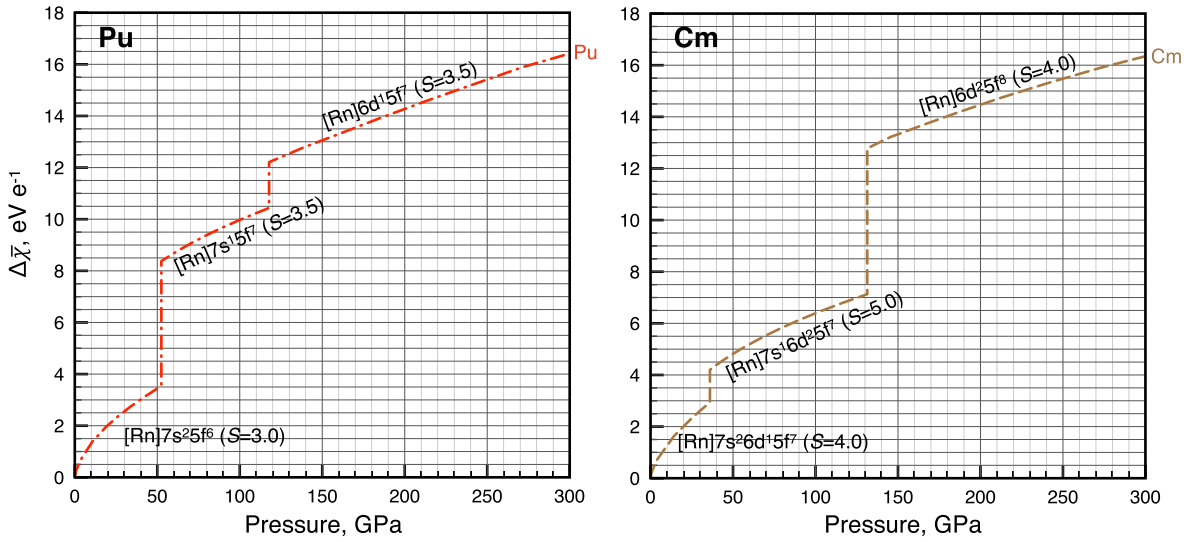

Figure 16. Change in average electron energy, $\Delta\bar{\chi}$, upon compression of row 7 f-block elements Pu and Cm relative to the atoms in vacuum. $\Delta\bar{\chi} > 0$ means electron destabilization, i.e., decreasing electronegativity. Pu is predicted to exhibit a unique 7s→5f transition.

for they are the only three atoms predicted to exhibit f→d demotions. This preference might be explained by reduced exchange repulsion concomitant with an increase in spin during the transition. This can be seen as a consequence of the Pauli exclusion principle acting to maximize magnetism, or alternatively, as a strengthening of Hund's rule under pressure relative to the *aufbau* principle. If this interpretation is correct, then only those atoms with an f-occupation equal to 8 or higher should be able to demonstrate pressure induced f→d demotions. We looked carefully at Er, Tm, Yb, and even Lu, but the energetics favoring pressure-induced f→d transitions appear unique to Tb, Dy, and Ho.

For Tb (Figure S11), the 1 atm ground state, $[Xe]6s^24f^9$ (S = 2.5), is predicted to undergo a three-electron restructuring into $[Xe]5d^34f^8$ (S = 5.0) at 43 GPa. For Ho, the same kind of transition, $[Xe]6s^24f^{11}$ (S = 1.5) → $[Xe]5d^34f^{10}$ (S = 3.5) is predicted at 61 GPa. For Dy, the f→d demotion, $[Xe]6s^24f^{10}$ (S = 2) → $[Xe]5d^34f^9$ (S = 4), is predicted at ∼54 GPa, and is followed by a "normal" one-electron $[Xe]5d^34f^9$ (S = 4) → $[Xe]5d^24f^{10}$ (S = 3) transition in the opposite direction at 115 GPa (Figure 15).

It appears that for Tb, Dy, and Ho a preference for magnetization (in a way, Hund's rule) can win out over the orbital-size effect governing pressure induced transitions in the rest of the periodic table. This prediction is amenable to experimental test. The preference is unexpected and predicts that, contrary to all other atoms, Tb, Dy, and Ho increase their electronegativity in a short span of pressures directly following their three-electron rearrangements (Figure 14).

As for the d-block elements, there are many ways in which the atomic lanthanide electronegativities might be used in explaining and predicting material properties. Figure 14 shows that, contrary to the first seven atoms of the lanthanides, the relative ordering of the last seven atoms (Gd−Yb) is predicted to be mostly reversed under compression. Gd remains one of the most electronegative lanthanide elements under compression. However, Tb and Ho are predicted to move up in the order and be the two most electronegative of the lanthanides at 300 GPa.

We turn finally to the last row of the (abbreviated) periodic table, the actinides. Cm is the heaviest atom for which our basis set is available. The atoms Th, U, and Np are omitted because calculations of competing configurations could not be sufficiently converged over the entire pressure range. Data for the remaining elements, Ac, Pa, Pu, Am, and Cm, are shown in Figures 16, 17, and S13. One of the oddities here is Pu, which

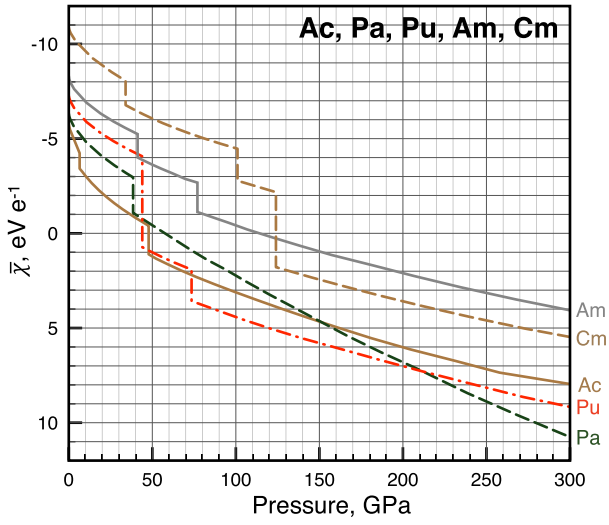

Figure 17. Compression of row 7 f-block elements Ac, Pa, Pu, Am, and Cm up to 300 GPa. Increasing average electron energy, $\Delta\bar{\chi}$, relative to the atom in vacuum is here offset by electronegativity tabulated under normal pressure conditions. As earlier, the y-scale is reversed so as to facilitate comparison of electronegativities, where up means more electronegative. Vertical jumps correspond to the electronic configurational transitions indicated in Figures 16 and S13.

is the only atom predicted to undergo a direct s→f transition. In Pu, this occurs at about 44 GPa, as the ground state $[Rn]7s^25f^6$ crosses with $[Rn]7s^15f^7$ and where the 5f shell becomes half-filled (Figure 16). The second crossing predicted at ∼74 GPa is instead s→d, into $[Rn]6d^15f^7$. In comparison, for Cm, the first transition from the ground state upon compression is s→d, corresponding to $[Rn]7s^26d^15f^7$ → $[Rn]7s^16d^25f^7$ at ∼34 GPa (Figure 16). The second crossing predicted at ∼100 GPa in Cm is also s→d, into $[Rn]6d^35f^7$.

DOI: 10.1021/jacs.9b02634
J. Am. Chem. Soc. 2019, 141, 10253−10271

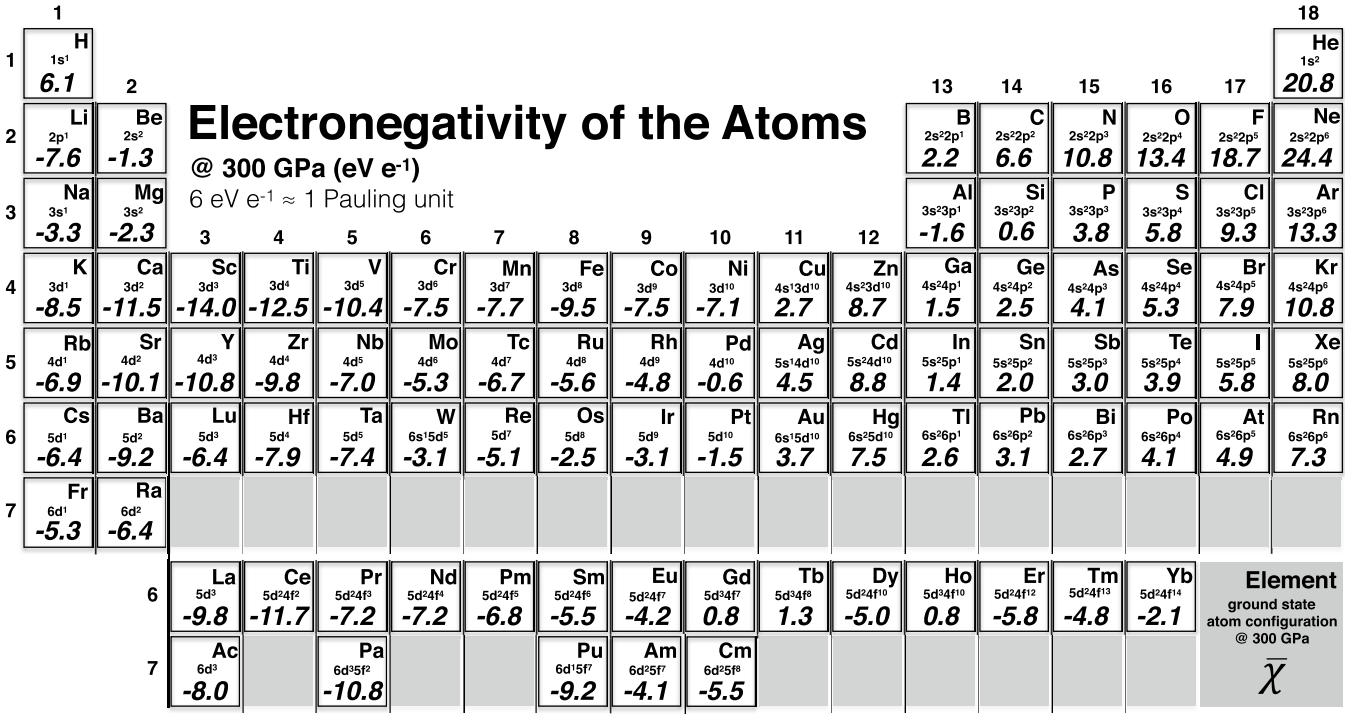

Figure 18. Electronegativity and predicted ground-state configuration of the atoms at 300 GPa. Increasing average electron energy, $\Delta\bar{\chi}_{0\rightarrow 300\ \mathrm{GPa}}$ relative to the atom in vacuum is here offset by electronegativity tabulated under normal pressure conditions.[102] The values are shown with a reversed sign such that more positive means more electronegative. Negative values correspond to average electron energies that lie above the external vacuum reference level. The listed electronegativity of Zn, Cd, and Hg is dependent on the choice of valence electron configuration used to define their ambient pressure electronegativity.[102] If instead of s^2d^{10} only the highest s level is used to define the valence of Zn, Cd, and Hg, their resulting electronegativities at 300 GPa becomes 2.2, 1.7, and 4.8 eV e^{-1}, respectively.

Finally, the third crossing in Cm is into $[Rn]6d^25f^8$ at 124 GPa. The behavior of Cm and Pu illustrates a close competition between a lower coulomb repulsion associated with d-occupation and a lower exchange repulsion associated with f-occupation. This competition can also be cast in the terminology of electronegativity, where configurations with more d-occupations correspond to a more electronegative atom at a given pressure. Notice, for instance the difference in magnitude of the electronegativity change in Pu for the s→d and the s→f transitions (Figures 16 and 17). In future work we will explore these fascinating state changes under compression in the actinides and lanthanides.

■ CONCLUSIONS

In this work we present a computational model capable of quantum mechanically studying compression of single atoms. The compression model has been validated against experimental equations of state of noble gas elements and describes isotropic compression of ground states ($T \rightarrow 0$ K) in a non-reactive environment, effectively neon-like. We have subjected 93 atoms to the compression model and predict changes to their ground-state electronic configurations at pressures ranging from 0 to 300 GPa. Our study confirms that the filling of energy levels in compressed atoms more closely follows the hydrogenic *aufbau* principle,[145,146] where the ordering is determined by the principal quantum number. In contrast, the Madelung energy ordering rule (that orbitals with a lower $n + l$ value are filled before orbitals with a higher $n + l$ value) is not predictive for atoms under compression. Magnetism may increase or decrease with pressure, depending which atom is considered. However, we find that Hund's rule is never violated for single atoms in the considered pressure range.

Changes in ground-state electronic configuration are a fact of life for compressed atoms, with important effects on properties. In this work we pay particular attention to the response of the average electron energy, $\bar{\chi}$, with compression. The negative of $\Delta\bar{\chi}$ is here defined as an atom's change in electronegativity upon compression, and this quantity can be used to predict changes to existing ambient pressure scales of electronegativity.

Our calculations of $\Delta\bar{\chi}$ are, in principle, subject to experimental verification. Dilute atoms trapped in a cryogenic noble gas matrix placed inside of a diamond anvil cell may allow for the photoelectron spectroscopy experiments necessary to measure the core and valence levels of compressed atoms.

Figure 18 shows the revised table of atomic electronegativity and ground-state configurations at one high pressure, 300 GPa. Note that in this final figure we are showing the negative of $\bar{\chi}$ to facilitate comparison with conventional electronegativity tables, where more positive means more electronegative. This snapshot at a single pressure captures the essence of this work. Our compression model predicts 300 GPa to lie in a pressure region devoid of configurational transitions in atoms (the nearest exception being Ce at 267 GPa). Under pressure, all electronegativities decrease. The physical reasoning for this decrease is given above. Three exceptions are Tb, Dy, and Ho, which show the opposite electronegativity trend in limited pressure ranges. The conversion factor of ~6 eV e^{-1} per Pauling unit might be kept in mind for the magnitude of the effect. Given the vacuum reference level, some of the

DOI: 10.1021/jacs.9b02634
J. Am. Chem. Soc. 2019, 141, 10253−10271

electronegativities actually become negative—there is nothing unphysical about this. It is the relative electronegativities—within a group, with other groups—that matter.

By and large, the main-group elements together with groups 11 and 12 have electronegativities ordered in the same fashion compared to lower pressures. The most electronegative element is Ne, followed by He and F. In contrast, all elements in groups 1−10 (except Pd), and all investigated lanthanides and actinides, are predicted to undergo ground-state conformational transitions below 300 GPa. For example, under sufficient compression the heavier members of groups 1 and 2 (K and heavier) should be considered part of the transition metal group. Numerous atoms also switch places in the ordering of electronegativity at different pressure intervals. As a consequence of this, Sc and Ti are, for example, predicted to be the least electronegative atoms at 300 GPa, by a sizable margin (Figure 18).

Because the ground-state configurations of most atoms and their electronegativities are radically different at higher pressures compared to atmospheric conditions, so will their chemistry be. For example, we have mentioned how the increased difference in electronegativity between Kr and O is one explanation for the predicted stability of KrO near 300 GPa.[132] Knowledge of changing ground states and increasing electronegativity differences might also be valuable for the rationalization of polyhydride stability and structure under pressure. We note, for example, that the largest electronegativity difference between H and any other atom at 300 GPa is a whopping 20.1 eV e^{-1} with Sc (Figure 18). Compressed scandium hydrides have been predicted to exhibit unusually high critical superconducting transition temperatures under compression.[147]

Multiple predicted crossings of electronegativity of atoms also suggest a tantalizing possibility of reversals in oxidation and reduction in different alloys. Such polarity reversals might be observable by X-ray diffraction and X-ray absorption experiments. Alternatively, the avoidance of such polarity reversals may prove an explanation for some pressure-induced phase transitions.

In conclusion, we believe the data presented herein extends our chemical intuition to higher pressures, can explain changed behavior in different thermodynamic regimes, and can act as a qualitative guide to both experiments and computational efforts.

■ ASSOCIATED CONTENT

Supporting Information

The Supporting Information is available free of charge on the ACS Publications website at DOI: 10.1021/jacs.9b02634.

Model comparison with experimental equations of state of the noble gas elements; tests of the dependence on the level of theory (PBE vs PBE0); effects of spin−orbit coupling; supplemental $\Delta\bar{\chi}$-plots and evolution of the ground-state configurations for several elements, and a table of the atoms showing $\Delta\bar{\chi}$ for compression to 300 GPa, including Figures S1−S15 (PDF)

■ AUTHOR INFORMATION

Corresponding Author

*martin.rahm@chalmers.se

ORCID

Martin Rahm: 0000-0001-7645-5923

Roald Hoffmann: 0000-0001-5369-6046

Notes

The authors declare no competing financial interest.

Our data set will become available for visualization in an interactive atomic database at www.rahmlab.com.

■ ACKNOWLEDGMENTS

We acknowledge funding from Chalmers University of Technology, the Energy Frontier Research in Extreme Environments (EFree) Center, an Energy Frontier Research Center funded by the U.S. Department of Energy, Office of Science, under Award Number DE-SC0001057, and the National Science Foundation (NSF) through Research Grant CHE 13-05872. This research relied on computational resources provided by the Swedish National Infrastructure for Computing (SNIC) at C3SE. Efflam Mercier is thanked for creating the Table of Contents graphic.

■ REFERENCES

(1) Grochala, W.; Hoffmann, R.; Feng, J.; Ashcroft, N. W. The chemical imagination at work in very tight places. *Angew. Chem., Int. Ed.* **2007**, *46*, 3620−3642.

(2) Eremets, M. I.; Gavriliuk, A. G.; Trojan, I. A.; Dzivenko, D. A.; Boehler, R. Single-bonded cubic form of nitrogen. *Nat. Mater.* **2004**, *3*, 558−563.

(3) Iota, V.; Yoo, C. S.; Cynn, H. Quartzlike carbon dioxide: An optically nonlinear extended solid at high pressures and temperatures. *Science* **1999**, *283*, 1510−1513.

(4) Drozdov, A. P.; Eremets, M. I.; Troyan, I. A.; Ksenofontov, V.; Shylin, S. I. Conventional superconductivity at 203 K at high pressures in the sulfur hydride system. *Nature* **2015**, *525*, 73−76.

(5) Fitzgibbons, T. C.; Guthrie, M.; Xu, E.-s.; Crespi, V. H.; Davidowski, S. K.; Cody, G. D.; Alem, N.; Badding, J. V. Benzene-derived carbon nanothreads. *Nat. Mater.* **2015**, *14*, 43−47.

(6) Dias, R. P.; Silvera, I. F. Observation of the Wigner-Huntington transition to metallic hydrogen. *Science* **2017**, *355*, 715−718.

(7) Zhang, L.; Wang, Y.; Lv, J.; Ma, Y. Materials discovery at high pressures. *Nat. Rev. Mater.* **2017**, *2*, 17005.

(8) Zurek, E.; Grochala, W. Predicting crystal structures and properties of matter under extreme conditions via quantum mechanics: the pressure is on. *Phys. Chem. Chem. Phys.* **2015**, *17*, 2917−2934.

(9) Fukui, K.; Yonezawa, T.; Shingu, H. A molecular-orbital theory of reactivity in aromatic hydrocarbons. *J. Chem. Phys.* **1952**, *20*, 722−725.

(10) Rahm, M.; Hoffmann, R.; Ashcroft, N. W. Atomic and Ionic Radii of Elements 1−96. *Chem. - Eur. J.* **2016**, *22*, 14625−14632.

(11) Allen, L. C. Extension and completion of the periodic table. *J. Am. Chem. Soc.* **1992**, *114*, 1510−1511.

(12) Rahm, M.; Hoffmann, R. Toward an Experimental Quantum Chemistry: Exploring a New Energy Partitioning. *J. Am. Chem. Soc.* **2015**, *137*, 10282−10291.

(13) Geerlings, P.; De Proft, F.; Langenaeker, W. Conceptual Density Functional Theory. *Chem. Rev.* **2003**, *103*, 1793−1873.

(14) Rahm, M.; Hoffmann, R. Distinguishing Bonds. *J. Am. Chem. Soc.* **2016**, *138*, 3731−3744.

(15) Anderson, J. S. M.; Melin, J.; Ayers, P. W. Conceptual Density-Functional Theory for General Chemical Reactions, Including Those That Are Neither Charge- nor Frontier-Orbital-Controlled. 1. Theory and Derivation of a General-Purpose Reactivity Indicator. *J. Chem. Theory Comput.* **2007**, *3*, 358−374.

(16) Politzer, P.; Murray, J. S.; Bulat, F. A. Average local ionization energy: a review. *J. Mol. Model.* **2010**, *16*, 1731−1742.

(17) Raccuglia, P.; Elbert, K. C.; Adler, P. D. F.; Falk, C.; Wenny, M. B.; Mollo, A.; Zeller, M.; Friedler, S. A.; Schrier, J.; Norquist, A. J. Machine-learning-assisted materials discovery using failed experiments. *Nature* **2016**, *533*, 73−76.

DOI: 10.1021/jacs.9b02634
J. Am. Chem. Soc. 2019, 141, 10253−10271

(18) Ward, L.; Agrawal, A.; Choudhary, A.; Wolverton, C. A general-purpose machine learning framework for predicting properties of inorganic materials. *Npj Comput. Mater.* **2016**, *2*, 16028.
(19) Krachmalnicoff, A.; Bounds, R.; Mamone, S.; Alom, S.; Concistre, M.; Meier, B.; Kouril, K.; Light, M. E.; Johnson, M. R.; Rols, S.; Horsewill, A. J.; Shugai, A.; Nagel, U.; Room, T.; Carravetta, M.; Levitt, M. H.; Whitby, R. J. The dipolar endofullerene HF@C60. *Nat. Chem.* **2016**, *8*, 953−957.
(20) Popov, A. A.; Yang, S.; Dunsch, L. Endohedral Fullerenes. *Chem. Rev.* **2013**, *113*, 5989−6113.
(21) Yeshchenko, O. A.; Dmitruk, I. M.; Koryakov, S. V.; Pundyk, I. P.; Barnakov, Y. A. Optical study of ZnP2 nanoparticles in zeolite Na-X. *Solid State Commun.* **2005**, *133*, 109−112.
(22) Tang, Z. K.; Nozue, Y.; Goto, T. Quantum size effect on the excited state of mercury diiodide, lead diiodide and bismuth triiodide clusters and molecules in zeolite LTA. *J. Phys. Soc. Jpn.* **1992**, *61*, 2943−2950.
(23) Bayer, M.; Stern, O.; Hawrylak, P.; Fafard, S.; Forchel, A. Hidden symmetries in the energy levels of excitonic 'artificial atoms'. *Nature (London, U. K.)* **2000**, *405*, 923−926.
(24) Wigner, E.; Seitz, F. Constitution of metallic sodium. *Phys. Rev.* **1933**, *43*, 804−810.
(25) Wigner, E.; Seitz, F. The constitution of metallic sodium. II. *Phys. Rev.* **1934**, *46*, 509−524.
(26) Michels, A.; de Boer, J.; Bijl, A. Molecular interaction and its influence on the polarizability. *Physica (Amsterdam)* **1937**, *4*, 981−994.
(27) Sommerfeld, A.; Welker, H. Künstliche Grenzbedingungen beim Keplerproblem. *Ann. Phys.* **1938**, *424*, 56−65.
(28) Sommerfeld, A.; Hartmann, H. Künstliche Grenzbedingungen in der Wellenmechanik. Der beschränkte Rotator. *Ann. Phys.* **1940**, *429*, 333−343.
(29) Ludena, E. V. SCF Hartree-Fock calculations of ground state wave functions of compressed atoms. *J. Chem. Phys.* **1978**, *69*, 1770−1775.
(30) de Groot, S. R.; Seldam, C. A. T. The energy levels of a model of the compressed hydrogen atom. *Physica (Amsterdam)* **1946**, *12*, 669−682.
(31) Fowler, P. W. Energy, polarizability and size of confined one-electron systems. *Mol. Phys.* **1984**, *53*, 865−889.
(32) Froeman, P. O.; Yngve, S.; Froeman, N. The energy levels and the corresponding normalized wave functions for a model of a compressed atom. *J. Math. Phys. (Melville, NY, U. S.)* **1987**, *28*, 1813−1826.
(33) Jaskolski, W. Confined many-electron systems. *Phys. Rep.* **1996**, *271*, 1−66.
(34) Lo, J. M. H.; Klobukowski, M.; Diercksen, G. H. F. Low-Lying Excited States of the Hydrogen Molecule in Cylindrical Harmonic Confinement. *Adv. Quantum Chem.* **2005**, *48*, 59−89.
(35) Cruz, S. A. Thomas-fermi-dirac-weizsacker density functional formalism applied to the study of many-electron atom confinement by open and closed boundaries. *Adv. Quantum Chem.* **2009**, *57*, 255−283.
(36) Sen, K. D.; Pupyshev, V. I.; Montgomery, H. E., Jr. Exact relations for confined one-electron systems. *Adv. Quantum Chem.* **2009**, *57*, 25−77.
(37) Dolmatov, V. K.; Baltenkov, A. S.; Connerade, J.-P.; Manson, S. T. Structure and photoionization of confined atoms. *Radiat. Phys. Chem.* **2004**, *70*, 417−433.
(38) Sil, A. N.; Canuto, S.; Mukherjee, P. K. Spectroscopy of confined atomic systems: effect of plasma. *Adv. Quantum Chem.* **2009**, *58*, 115−175.
(39) Garza, J.; Vargas, R.; Sen, K. D. Electronic structure of confined atoms. *Chem. React. Theory* **2009**, 521−537.
(40) Sen, K. D. *Electronic Structure of Quantum Confined Atoms and Molecules*; Springer, 2014.
(41) Connerade, J. P.; Semaoune, R. Atomic compressibility and reversible insertion of atoms into solids. *J. Phys. B: At., Mol. Opt. Phys.* **2000**, *33*, 3467−3484.
(42) Connerade, J. P.; Dolmatov, V. K.; Lakshmi, P. A. The filling of shells in compressed atoms. *J. Phys. B: At., Mol. Opt. Phys.* **2000**, *33*, 251−264.
(43) Dong, X.; Oganov, A. R.; Qian, G.; Zhou, X.-F.; Zhu, Q.; Wang, H.-T. How do chemical properties of the atoms change under pressure? *arXiv:1503.00230 [cond-mat.mtrl-sci]*, **2015**
(44) Miao, M.-S.; Hoffmann, R. High Pressure Electrides: A Predictive Chemical and Physical Theory. *Acc. Chem. Res.* **2014**, *47*, 1311−1317.
(45) Spooner, J.; Smith, B.; Weinberg, N. Effect of high pressure on the topography of potential energy surfaces. *Can. J. Chem.* **2016**, *94*, 1057−1064.
(46) Cammi, R. A new extension of the polarizable continuum model: Toward a quantum chemical description of chemical reactions at extreme high pressure. *J. Comput. Chem.* **2015**, *36*, 2246−2259.
(47) Cammi, R. Quantum Chemistry at the High Pressures: The eXtreme Pressure Polarizable Continuum Model (XP-PCM). In *Frontiers of Quantum Chemistry*; Wojcik, M. J., Nakatsuji, H., Kirtman, B., Ozaki, Y.,, Eds.; Springer, 2018; pp 273−287.
(48) Lundqvist, S.; March, N. H. *Theory of the Inhomogeneous Electron Gas*; Springer: Boston, MA, 1983.
(49) Rousseau, B.; Ashcroft, N. W. Interstitial electronic localization. *Phys. Rev. Lett.* **2008**, *101*, 046407.
(50) Alchagirov, A. B.; Perdew, J. P.; Boettger, J. C.; Albers, R. C.; Fiolhais, C. Energy and pressure versus volume: Equations of state motivated by the stabilized jellium model. *Phys. Rev. B: Condens. Matter Mater. Phys.* **2001**, *63*, 224115.
(51) Holzapfel, W. B. Energy and pressure versus volume: equations of state motivated by the stabilized jellium model. Comment. *Phys. Rev. B: Condens. Matter Mater. Phys.* **2003**, *67*, 026102.
(52) Tomasi, J.; Mennucci, B.; Cammi, R. Quantum Mechanical Continuum Solvation Models. *Chem. Rev.* **2005**, *105*, 2999−3093.
(53) Amovilli, C.; Mennucci, B. Self-Consistent Field Calculation of Pauli Repulsion and Dispersion Contributions to the Solvation Free Energy in the Polarizable Continuum Model. *J. Phys. Chem. B* **1997**, *101*, 1051−1057.
(54) Cammi, R. *Molecular response functions for the Polarizable Continuum Model: physical basis and Quantum Mechanical formalism*; Springer Verlag: Heidelberg, 2013.
(55) Cammi, R.; Chen, B.; Rahm, M. Analytical calculation of pressure for confined atomic and molecular systems using the eXtreme-Pressure Polarizable Continuum Model. *J. Comput. Chem.* **2018**, *39*, 2243−2250.
(56) Hellmann, H. *Einführung in die Quantenchemie*; Franz Deuticke: Leipzig, 1937; p 285.
(57) Feynman, R. P. Forces in molecules. *Phys. Rev.* **1939**, *56*, 340−343.
(58) Cammi, R. The virial theorem for the polarizable continuum model. *J. Chem. Phys.* **2014**, *140*, 084112.
(59) Alvarez, S. A cartography of the van der Waals territories. *Dalton Trans.* **2013**, *42*, 8617−8636.
(60) Vogt, J.; Alvarez, S. van der Waals Radii of Noble Gases. *Inorg. Chem.* **2014**, *53*, 9260−9266.
(61) Fukuda, R.; Ehara, M.; Cammi, R. Modeling Molecular Systems at Extreme Pressure by an Extension of the Polarizable Continuum Model (PCM) Based on the Symmetry-Adapted Cluster-Configuration Interaction (SAC-CI) Method: Confined Electronic Excited States of Furan as a Test Case. *J. Chem. Theory Comput.* **2015**, *11*, 2063−2076.
(62) Cammi, R.; Cappelli, C.; Mennucci, B.; Tomasi, J. Calculation and analysis of the harmonic vibrational frequencies in molecules at extreme pressure: methodology and diborane as a test case. *J. Chem. Phys.* **2012**, *137*, 154112.
(63) Pagliai, M.; Cardini, G.; Cammi, R. Vibrational Frequencies of Fullerenes C60 and C70 under Pressure Studied with a Quantum Chemical Model Including Spatial Confinement Effects. *J. Phys. Chem. A* **2014**, *118*, 5098−5111.
(64) XP-PCM, F. The p = 1 GPa reference is used only for our validation when comparing to experimental equations of state (V/

DOI: 10.1021/jacs.9b02634
J. Am. Chem. Soc. 2019, 141, 10253−10271

V1). p = 1 GPa is an arbitrary choice, but one that is motivated by a large volume change below 1 GPa. Experimental volumes at lower pressures are more dependent on temperature, and our method needed to be validated for higher pressures.
(65) Young, D. A.; Cynn, H.; Söderlind, P.; Landa, A. Zero-Kelvin Compression Isotherms of the Elements 1 ≤ Z ≤ 92 to 100 GPa. *J. Phys. Chem. Ref. Data* **2016**, *45*, 043101.
(66) Martinez-Sanchez, M.-A.; Rodriguez-Bautista, M.; Vargas, R.; Garza, J. Solution of the Kohn-Sham equations for many-electron atoms confined by penetrable walls. *Theor. Chem. Acc.* **2016**, *135*, 1−10.
(67) Rodriguez-Bautista, M.; Diaz-Garcia, C.; Navarrete-Lopez, A. M.; Vargas, R.; Garza, J. Roothaan's approach to solve the Hartree-Fock equations for atoms confined by soft walls: Basis set with correct asymptotic behavior. *J. Chem. Phys.* **2015**, *143*, 034103.
(68) Sarsa, A.; Buendia, E.; Galvez, F. J. Study of confined many electron atoms by means of the POEP method. *J. Phys. B: At., Mol. Opt. Phys.* **2014**, *47*, 185002.
(69) Garza, J.; Hernandez-Perez, J. M.; Ramirez, J.-Z.; Vargas, R. Basis set effects on the Hartree-Fock description of confined many-electron atoms. *J. Phys. B: At., Mol. Opt. Phys.* **2012**, *45*, 015002.
(70) Adamo, C.; Barone, V. Toward reliable density functional methods without adjustable parameters: the PBE0 model. *J. Chem. Phys.* **1999**, *110*, 6158−6170.
(71) Douglas, M.; Kroll, N. M. Quantum electrodynamical corrections to the fine structure of helium. *Ann. Phys. (Amsterdam, Neth.)* **1974**, *82*, 89−155.
(72) Hess, B. A. Applicability of the no-pair equation with free-particle projection operators to atomic and molecular structure calculations. *Phys. Rev. A: At., Mol., Opt. Phys.* **1985**, *32*, 756−763.
(73) Hess, B. A. Relativistic electronic-structure calculations employing a two-component no-pair formalism with external-field projection operators. *Phys. Rev. A: At., Mol., Opt. Phys.* **1986**, *33*, 3742−3748.
(74) Barysz, M.; Sadlej, A. J. Two-component methods of relativistic quantum chemistry: from the Douglas-Kroll approximation to the exact two-component formalism. *J. Mol. Struct.: THEOCHEM* **2001**, *573*, 181−200.
(75) de Jong, W. A.; Harrison, R. J.; Dixon, D. A. Parallel Douglas-Kroll energy and gradients in NWChem: Estimating scalar relativistic effects using Douglas-Kroll contracted basis sets. *J. Chem. Phys.* **2001**, *114*, 48−53.
(76) Widmark, P. O.; Malmqvist, P.; Roos, B. O. Density matrix averaged atomic natural orbital (ANO) basis sets for correlated molecular wave functions. I. First row atoms. *Theor. Chim. Acta* **1990**, *77*, 291−306.
(77) Roos, B. O.; Veryazov, V.; Widmark, P. Relativistic atomic natural orbital type basis sets for the alkaline and alkaline-earth atoms applied to the ground-state potentials for the corresponding dimers. *Theor. Chem. Acc.* **2004**, *111*, 345−351.
(78) Roos, B. O.; Lindh, R.; Malmqvist, P.-å.; Veryazov, V.; Widmark, P. Main Group Atoms and Dimers Studied with a New Relativistic ANO Basis Set. *J. Phys. Chem. A* **2004**, *108*, 2851−2858.
(79) Roos, B. O.; Lindh, R.; Malmqvist, P.-A.; Veryazov, V.; Widmark, P. New Relativistic ANO Basis Sets for Transition Metal Atoms. *J. Phys. Chem. A* **2005**, *109*, 6575−6579.
(80) Roos, B. O.; Lindh, R.; Malmqvist, P.-A.; Veryazov, V.; Widmark, P. New relativistic ANO basis sets for actinide atoms. *Chem. Phys. Lett.* **2005**, *409*, 295−299.
(81) Roos, B. O.; Lindh, R.; Malmqvist, P.; Veryazov, V.; Widmark, P.; Borin, A. C. New Relativistic Atomic Natural Orbital Basis Sets for Lanthanide Atoms with Applications to the Ce Diatom and LuF3. *J. Phys. Chem. A* **2008**, *112*, 11431−11435.
(82) Pauling, L. Nature of the chemical bond. IV. The energy of single bonds and the relative electronegativity of atoms. *J. Am. Chem. Soc.* **1932**, *54*, 3570−3582.
(83) Mulliken, R. S. New electroaffinity scale; together with data on valence states and on valence ionization potentials and electron affinities. *J. Chem. Phys.* **1934**, *2*, 782−793.
(84) Gordy, W. A new method of determining electronegativity from other atomic properties. *Phys. Rev.* **1946**, *69*, 604−607.
(85) Walsh, A. D. Factors Affecting Bond Strengths. I. A Possible New Definition of Electronegativity. *Proc. R. Soc. London, Ser. A* **1951**, *207*, 13−22.
(86) Sanderson, R. T. An interpretation of bond lengths and a classification of bonds. *Science* **1951**, *114*, 670−672.
(87) Allred, A. L.; Rochow, E. G. A scale of electronegativity based on electrostatic force. *J. Inorg. Nucl. Chem.* **1958**, *5*, 264−268.
(88) Iczkowski, R. P.; Margrave, J. L. Electronegativity. *J. Am. Chem. Soc.* **1961**, *83*, 3547−3551.
(89) Sanderson, R. T. Electronegativity and bond energy. *J. Am. Chem. Soc.* **1983**, *105*, 2259−2261.
(90) Pearson, R. G. Absolute electronegativity and absolute hardness of Lewis acids and bases. *J. Am. Chem. Soc.* **1985**, *107*, 6801−6806.
(91) Allen, L. C. Electronegativity is the average one-electron energy of the valence-shell electrons in ground-state free atoms. *J. Am. Chem. Soc.* **1989**, *111*, 9003−9014.
(92) Reed, J. L. Electronegativity: an atom in a molecule. *J. Phys. Chem.* **1991**, *95*, 6866−6870.
(93) Ghosh, D. C. A new scale of electronegativity based on absolute radii of atoms. *J. Theor. Comput. Chem.* **2005**, *4*, 21−33.
(94) Putz, M. V. Systematic formulations for electronegativity and hardness and their atomic scales within density functional softness theory. *Int. J. Quantum Chem.* **2006**, *106*, 361−389.
(95) Politzer, P.; Peralta-Inga Shields, Z.; Bulat, F. A.; Murray, J. S. Average Local Ionization Energies as a Route to Intrinsic Atomic Electronegativities. *J. Chem. Theory Comput.* **2011**, *7*, 377−384.
(96) Politzer, P.; Murray, J. S. Electronegativity—a perspective. *J. Mol. Model.* **2018**, *24*, 214.
(97) Ferro-Costas, D.; Perez-Juste, I.; Mosquera, R. A. Electronegativity estimator built on QTAIM-based domains of the bond electron density. *J. Comput. Chem.* **2014**, *35*, 978−985.
(98) Boyd, R. J.; Edgecombe, K. E. Atomic and group electronegativities from the electron-density distributions of molecules. *J. Am. Chem. Soc.* **1988**, *110*, 4182−4186.
(99) Boyd, R. J.; Boyd, S. L. Group electronegativities from the bond critical point model. *J. Am. Chem. Soc.* **1992**, *114*, 1652−1655.
(100) Jensen, W. B. Electronegativity from Avogadro to Pauling. Part I: origins of the electronegativity concept. *J. Chem. Educ.* **1996**, *73*, 11−20.
(101) Jensen, W. B. Electronegativity from Avogadro to Pauling: II. Late nineteenth- and early twentieth-century developments. *J. Chem. Educ.* **2003**, *80*, 279−287.
(102) Rahm, M.; Zeng, T.; Hoffmann, R. Electronegativity Seen as the Ground-State Average Valence Electron Binding Energy. *J. Am. Chem. Soc.* **2019**, *141*, 342−351.
(103) Allen, L. C. Chemistry and electronegativity. *Int. J. Quantum Chem.* **1994**, *49*, 253−277.
(104) Mann, J. B.; Meek, T. L.; Allen, L. C. Configuration Energies of the Main Group Elements. *J. Am. Chem. Soc.* **2000**, *122*, 2780−2783.
(105) Weisskopf, V. F. Search for Simplicity: Quantum mechanics and the Pauli principle. *Am. J. Phys.* **1985**, *53*, 109−110.
(106) Sessler, C. D.; Rahm, M.; Becker, S.; Goldberg, J. M.; Wang, F.; Lippard, S. J. CF2H, a Hydrogen Bond Donor. *J. Am. Chem. Soc.* **2017**, *139*, 9325−9332.
(107) Parr, R. G.; Donnelly, R. A.; Levy, M.; Palke, W. E. Electronegativity: The density functional viewpoint. *J. Chem. Phys.* **1978**, *68*, 3801−3807.
(108) Lozano-Espinosa, M.; Garza, J.; Galvan, M. Confinement effects on the spin potential of first row transition metal cations. *Philos. Mag.* **2017**, *97*, 284−297.
(109) Kuemmel, S.; Kronik, L. Orbital-dependent density functionals: Theory and applications. *Rev. Mod. Phys.* **2008**, *80*, 3−60.
(110) McAdon, M. H.; Goddard, W. A. New Concepts of Metallic Bonding Based on Valence-Bond Ideas. *Phys. Rev. Lett.* **1985**, *55*, 2563−2566.

DOI: 10.1021/jacs.9b02634
J. Am. Chem. Soc. 2019, 141, 10253−10271

(111) McAdon, M. H.; Goddard, W. A. Generalized valence bond studies of metallic bonding: naked clusters and applications to bulk metals. *J. Phys. Chem.* **1987**, *91*, 2607−2626.
(112) Boettger, J. C.; Trickey, S. B. Equation of state and properties of lithium. *Phys. Rev. B: Condens. Matter Mater. Phys.* **1985**, *32*, 3391−3398.
(113) Neaton, J. B.; Ashcroft, N. W. Pairing in dense lithium. *Nature* **1999**, *400*, 141−144.
(114) Hanfland, M.; Syassen, K.; Christensen, N. E.; Novikov, D. L. New high-pressure phases of lithium. *Nature* **2000**, *408*, 174−174.
(115) Rousseau, R.; Uehara, K.; Klug, D. D.; Tse, J. S. Phase Stability and Broken-Symmetry Transition of Elemental Lithium up to 140 GPa. *ChemPhysChem* **2005**, *6*, 1703−1706.
(116) Naumov, I. I.; Hemley, R. J.; Hoffmann, R.; Ashcroft, N. W. Chemical bonding in hydrogen and lithium under pressure. *J. Chem. Phys.* **2015**, *143*, 064702.
(117) Huzinaga, S.; Andzelm, J.; Radzio-Andzelm, E.; Sakai, Y.; Tatewaki, H.; Klobukowski, M. *Gaussian Basis Sets for Molecular Calculations*; Elsevier Science: Amsterdam, 1983.
(118) Sternheimer, R. M. The compressibility of metallic cesium. *Phys. Rev.* **1950**, *78*, 235−243.
(119) Hooper, J.; Zurek, E. High Pressure Potassium Polyhydrides: A Chemical Perspective. *J. Phys. Chem. C* **2012**, *116*, 13322−13328.
(120) Zurek, E. Hydrides of the Alkali Metals and Alkaline Earth Metals Under Pressure. *Comments Inorg. Chem.* **2017**, *37*, 78−98.
(121) Zhou, D.; Jin, X.; Meng, X.; Bao, G.; Ma, Y.; Liu, B.; Cui, T. Ab initio study revealing a layered structure in hydrogen-rich KH6 under high pressure. *Phys. Rev. B: Condens. Matter Mater. Phys.* **2012**, *86*, 014118.
(122) Botana, J.; Miao, M.-S. Pressure-stabilized lithium caesides with caesium anions beyond the −1 state. *Nat. Commun.* **2014**, *5*, 4861.
(123) Miao, M.-s. Caesium in high oxidation states and as a p-block element. *Nat. Chem.* **2013**, *5*, 846−852.
(124) Olijnyk, H.; Holzapfel, W. B. Phase transitions in alkaline earth metals under pressure. *Phys. Lett. A* **1984**, *100A*, 191−194.
(125) Pickard, C. J.; Needs, R. J. Predicted pressure-induced s-band ferromagnetism in alkali metals. *Phys. Rev. Lett.* **2011**, *107*, 087201.
(126) Dong, S.; Zhao, H. Pressure-induced ferromagnetism in open structure alkali metals from first principles. *Appl. Phys. Lett.* **2012**, *100*, 142404.
(127) Matsushita, M.; Endo, S.; Miura, K.; Ono, F. Pressure induced magnetic phase transition in Fe-Ni Invar alloy. *J. Magn. Magn. Mater.* **2003**, *265*, 352−356.
(128) Petrillo, C.; Postorino, P.; Orecchini, A.; Sacchetti, F. Search for the elusive magnetic state of hexagonal iron: The antiferromagnetic Fe71Ru29 hcp. alloy. *J. Magn. Magn. Mater.* **2018**, *449*, 552−557.
(129) Steinle-Neumann, G.; Stixrude, L.; Cohen, R. E. Magnetism in dense hexagonal iron. *Proc. Natl. Acad. Sci. U. S. A.* **2004**, *101*, 33.
(130) Freiman, Y. A.; Jodl, H. J.; Crespo, Y. Solid oxygen revisited. *Phys. Rep.* **2018**, *743*, 1−55.
(131) Klotz, S. Magnetism in Solid Oxygen Studied by High-Pressure Neutron Diffraction. *J. Low Temp. Phys.* **2018**, *192*, 1−18.
(132) Zaleski-Ejgierd, P.; Lata, P. M. Krypton oxides under pressure. *Sci. Rep.* **2016**, *6*, 18938−18938.
(133) Miao, M.-s.; Wang, X.-l.; Brgoch, J.; Spera, F.; Jackson, M. G.; Kresse, G.; Lin, H.-q. Anionic Chemistry of Noble Gases: Formation of Mg−NG (NG = Xe, Kr, Ar) Compounds under Pressure. *J. Am. Chem. Soc.* **2015**, *137*, 14122−14128.
(134) Kutzelnigg, W.; Morgan, J. D., III. Hund's rules. *Z. Phys. D: At., Mol. Clusters* **1996**, *36*, 197−214.
(135) Kollmar, H.; Staemmler, V. Violation of Hund's rule by spin polarization in molecules. *Theor. Chim. Acta* **1978**, *48*, 223−239.
(136) Hrovat, D. A.; Borden, T. Violations of Hund's rule in molecules - where to look for them and how to identify them. *J. Mol. Struct.: THEOCHEM* **1997**, *398*−*399*, 211−220.
(137) Mock, M. T.; Chen, S.; Rousseau, R.; O'Hagan, M. J.; Dougherty, W. G.; Kassel, W. S.; DuBois, D. L.; Bullock, R. M. A rare terminal dinitrogen complex of chromium. *Chem. Commun. (Cambridge, U. K.)* **2011**, *47*, 12212−12214.
(138) He, L.; Bester, G.; Zunger, A. Electronic Phase Diagrams of Carriers in Self-Assembled Quantum Dots: Violation of Hund's Rule and the Aufbau Principle for Holes. *Phys. Rev. Lett.* **2005**, *95*, 246804.
(139) Sheng, W.; Sun, M.; Zhou, A. Violation of Hund's rule and quenching of long-range electron-electron interactions in graphene nanoflakes. *Phys. Rev. B: Condens. Matter Mater. Phys.* **2013**, *88*, 085432.
(140) Ashcroft, N. W. Hydrogen Dominant Metallic Alloys: High Temperature Superconductors? *Phys. Rev. Lett.* **2004**, *92*, 187002.
(141) Osman, H. H.; Salvado, M. A.; Pertierra, P.; Engelkemier, J.; Fredrickson, D. C.; Recio, J. M. Chemical Pressure Maps of Molecules and Materials: Merging the Visual and Physical in Bonding Analysis. *J. Chem. Theory Comput.* **2018**, *14*, 104−114.
(142) Zhu, L.; Liu, H.; Pickard, C. J.; Zou, G.; Ma, Y. Reactions of xenon with iron and nickel are predicted in the Earth's inner core. *Nat. Chem.* **2014**, *6*, 644−648.
(143) Dewaele, A.; Pépin, C. M.; Geneste, G.; Garbarino, G. Reaction between nickel or iron and xenon under high pressure. *High Pressure Res.* **2017**, *37*, 137−146.
(144) Nakano, H.; Uchiyama, R.; Hirao, K. Quasi-degenerate perturbation theory with general multiconfiguration self-consistent field reference functions. *J. Comput. Chem.* **2002**, *23*, 1166−1175.
(145) Bohr, N. *The Theory of Spectra and Atomic Constitution*; Cambridge Universtity Press: Cambridge, UK, 1922.
(146) Stoner, E. C. LXXIII. The distribution of electrons among atomic levels. *London, Edinburgh, Dublin Philos. Mag. J. Sci.* **1924**, *48*, 719−736.
(147) Ye, X.; Zarifi, N.; Zurek, E.; Hoffmann, R.; Ashcroft, N. W. High Hydrides of Scandium under Pressure: Potential Superconductors. *J. Phys. Chem. C* **2018**, *122*, 6298−6309.
(148) (a) Batsanov, S. S. Effect of high pressure on crystal electronegativities of elements. *J. Phys. Chem. Solids* **1997**, *58*, 527−532. (b) Van Vechten, J. A. Quantum dielectric theory of electronegativity in covalent systems. I. Electronic dielectric constant. *Phys. Rev.* **1969**, *182*, 891−905.
(149) Parker, L. J.; Atou, T.; Badding, J. V. Transition Element-Like Chemistry for Potassium Under Pressure. *Science* **1996**, *273*, 95−97.
(150) Atou, T.; Hasegawa, M.; Parker, L. J.; Badding, J. V. Unusual Chemical Behavior for Potassium under Pressure: Potassium-Silver Compounds. *J. Am. Chem. Soc.* **1996**, *118*, 12104−12108.

NOTE ADDED IN PROOF

We have become aware of a body of work by Batsanov (a leading reference is 148a) and Van Vechten (a leading reference is 148b) on the effect of pressure on electronegativity, and of the Badding group on high pressure chemistry of potassium (two references, 149 and 150).

DOI: 10.1021/jacs.9b02634
J. Am. Chem. Soc. 2019, 141, 10253−10271